

## ARTICLE OPEN



# Reduced excitatory activity in the developing mPFC mediates a PV<sub>H</sub>-to-PV<sub>L</sub> transition and impaired social cognition in autism spectrum disorders

Yujian Luo<sup>1,2,7</sup>, Liangliang Wang<sup>1,3,7</sup>, Yirong Cao<sup>4,5</sup>, Ying Shen<sup>6</sup>, Yan Gu<sup>4,5</sup>✉ and Lang Wang<sup>1,2</sup>✉

© The Author(s) 2024

Understanding the neuropathogenesis of impaired social cognition in autism spectrum disorders (ASD) is challenging. Altered cortical parvalbumin-positive (PV<sup>+</sup>) interneurons have been consistently observed in ASD, but their roles and the underlying mechanisms remain poorly understood. In our study, we observed a downward-shifted spectrum of PV expression in the developing medial prefrontal cortex (mPFC) of ASD mouse models due to decreased activity of PV<sup>+</sup> neurons. Surprisingly, chemogenetically suppressing PV<sup>+</sup> neuron activity during postnatal development failed to induce ASD-like behaviors. In contrast, lowering excitatory activity in the developing mPFC not only dampened the activity state and PV expression of individual PV<sup>+</sup> neurons, but also replicated ASD-like social deficits. Furthermore, enhancing excitation, but not PV<sup>+</sup> interneuron-mediated inhibition, rescued social deficits in ASD mouse models. Collectively, our findings propose that reduced excitatory activity in the developing mPFC may serve as a shared local circuitry mechanism triggering alterations in PV<sup>+</sup> interneurons and mediating impaired social functions in ASD.

*Translational Psychiatry* (2024)14:325; <https://doi.org/10.1038/s41398-024-03043-2>

## INTRODUCTION

The etiology of autism spectrum disorders (ASD) has been extensively studied at the molecular, synaptic, and circuit levels [1–5]. Previous research has proposed several hypotheses to explain the neuropathogenesis of ASD, such as the imbalance between excitation and inhibition (E/I) in local cortical microcircuits [6, 7] or the functional disconnection between high cognitive function-related brain regions [8]. However, it remains confusing and controversial whether there is a common neurobiological basis for the core symptoms in ASD, such as social cognitive deficits.

The prefrontal cortex, especially the medial prefrontal cortex (mPFC), has been shown highly involved in social behaviors [9, 10]. Dysfunction of the mPFC has been commonly linked with social cognitive deficits [11]. The physiological roles of parvalbumin-positive (PV<sup>+</sup>) inhibitory interneurons in the mPFC have been intensely studied due to their large number, broad connectivity, and distinct firing pattern [12]. Previous research has consistently identified changes in PV<sup>+</sup> interneurons in both ASD patients and animal models [13, 14], including a reduction in density, PV expression, and neuronal activity. However, the mechanisms underlying these changes in PV<sup>+</sup> neurons in ASD are not well understood. Moreover, it remains to be determined whether there is a causal link between the dysfunction of mPFC PV<sup>+</sup> neurons

during early postnatal development and impaired social functions later.

In this study, using two distinct ASD mouse models, we observed that decreased excitatory activity resulted in a down-regulation of PV<sup>+</sup> neuron activity in the developing mPFC, leading to a distinct shift in the spectrum of PV expression. This shift was characterized by a consistent transition from neurons with high-level PV expression (PV<sub>H</sub>) to neurons with low-level PV expression (PV<sub>L</sub>). Selectively suppressing excitatory activity in the developing mPFC not only led to a PV<sub>H</sub>-to-PV<sub>L</sub> transition, but also replicated ASD-like social novelty deficit. Moreover, enhancing excitatory activity in the mPFC effectively rescued social novelty deficit in different ASD mouse models, whereas enhancing PV<sup>+</sup> interneuron-mediated inhibitory activity in the mPFC did not produce the same results. Together, our results demonstrate that reduced excitatory activity in the developing mPFC may represent a common local circuitry mechanism which triggers the alterations in PV<sup>+</sup> interneurons and mediates impaired social functions in ASD.

## MATERIALS AND METHODS

### Animals

Experiments were performed using wild-type C57BL/6J mice, unless otherwise mentioned. PV-Cre (Stock No. 008069) and Fmr1-KO (Stock No.

<sup>1</sup>Department of Neurology of the First Affiliated Hospital, Interdisciplinary Institute of Neuroscience and Technology, Zhejiang University School of Medicine, Hangzhou, China.

<sup>2</sup>School of Brain Science and Brain Medicine, Zhejiang University, Hangzhou, China. <sup>3</sup>Department of Psychiatry, Sir Run Run Shaw Hospital, Zhejiang University School of Medicine, Hangzhou, China. <sup>4</sup>Center of Stem Cell and Regenerative Medicine, and Department of Neurology of the Second Affiliated Hospital, NHC and CAMS Key Laboratory of Medical Neurobiology, Zhejiang University School of Medicine, Hangzhou, China. <sup>5</sup>MOE Frontier Science Center for Brain Science & Brain-Machine Integration, Zhejiang University, Hangzhou, China. <sup>6</sup>Department of Physiology and Department of Psychiatry, Sir Run Run Shaw Hospital, Zhejiang University School of Medicine, Hangzhou, China.

<sup>7</sup>These authors contributed equally: Yujian Luo, Liangliang Wang. ✉email: [guyan2015@zju.edu.cn](mailto:guyan2015@zju.edu.cn); [wanglang@zju.edu.cn](mailto:wanglang@zju.edu.cn)

Received: 10 April 2024 Revised: 17 July 2024 Accepted: 29 July 2024

Published online: 06 August 2024

003024) mice were from Jackson Labs. All procedures were approved by the Animal Care and Use Committee of Zhejiang University School of Medicine, and conducted in accordance with the policies of institutional guidelines on the care and use of laboratory animals. All animals were maintained a 12-h light/12-h dark cycle in a temperature-controlled (22–24 °C) room, group-housed (3–4 per cage) with free access to normal food and water. Both male and female mice were used for experiments.

### Preparation of VPA-exposed mice

VPA-exposed mice (VPA mice) were generated by administering VPA to pregnant mice at gestational age of 12.5 days (E12.5), as previously described [15]. Briefly, sodium salt of VPA (Sigma-Aldrich, P4543) was dissolved in sterile saline to a concentration of 50 mg/ml. Pregnant mice received a single intraperitoneal (i.p.) injection of VPA solution at a dose of 500 mg/kg at E12.5. Control mice were administered with sterile saline of the same volume at the same gestational age. The offspring of VPA- or saline-treated mice were used for experiments.

### Immunostaining

Mice were deeply anesthetized and then transcardially perfused with 0.1M PBS (pH 7.2) followed by 4% PFA. Brains were then post-fixed in 4% PFA overnight and then transferred to 30% (w/v) sucrose solution and stored at 4 °C. Brains were sectioned into 40 µm coronal sections using a microtome (Leica SM2010R). Brain sections containing the mPFC were permeabilized and blocked with phosphate buffered saline (PBS) containing 0.25% (w/v) Triton-X 100 and 2.5% normal donkey serum. Regular immunohistochemistry was then performed using primary antibodies overnight at 4 °C, followed by incubation with secondary antibodies for 2 h at room temperature (25 °C), in the presence of 2.5% donkey serum, 1% bovine serum albumin and 0.25% Triton X-100. Primary antibodies used in the present study included rabbit anti-PV (Abcam, ab11427, 1:1000), mouse anti-PV (Swant, 235, 1:2000), mouse anti-GAD67 (Millipore, MAB5406, 1:500), rabbit anti-c-Fos (Synaptic Systems, 226008, 1:3000), guinea pig anti-c-Fos (Synaptic Systems, 226308, 1:3000) and goat anti-mCherry (SIGGEN, AB0040-200, 1:3000). Secondary antibodies used in this study were donkey anti-rabbit Cy2, donkey anti-mouse Cy2, donkey anti-rabbit Cy3, donkey anti-mouse Cy3, donkey anti-goat Cy3, donkey anti-rabbit Cy5, donkey anti-mouse Cy5, donkey anti-guinea pig Cy5 (Jackson ImmunoResearch Lab, 711-225-152, 715-225-151, 711-165-152, 715-165-151, 705-165-147, 711-175-152, 715-175-151, 706-175-148, 1:1000). Stained sections were mounted on slides with Fluoromount-G anti-fade medium containing DAPI (Southern Biotech, 0100-20).

### BrdU labeling and staining

Embryonic BrdU labeling was performed as described previously [16]. A single BrdU injection was performed intraperitoneally to pregnant mice at embryonic day 11.5 (E11.5), 13.5 (E13.5), or 15.5 (E15.5). The offspring were perfused at desired time points, and the mPFC brain sections were pretreated with acid before immunostaining. Briefly, the slices were incubated in 1 N HCl for 25 min at 37 °C, followed by 10 min incubation in sodium borate buffer (pH 8.0). Brain sections were then washed with PBS and regular immunohistochemistry was performed afterwards using a primary antibody rat anti-BrdU (Abcam, ab6326, 1:1000) and a secondary antibody donkey anti-rat Cy2 (Jackson ImmunoResearch Lab, 1:1000).

### Imaging and analysis

Images of z stacks covering a thickness of  $25.5 \pm 1.5$  µm of the brain sections were taken on an Olympus FV3000 confocal microscope (Olympus, Japan), with a step size of 1 µm. Images were then analyzed using Image J or Imaris × 64 9.0.1. For imaging the PV immunoreactivity intensity, the imaging parameters were set using sections from P21 control mice, and then used on sections from all other animals. The PV immunoreactivity intensity of PV<sup>+</sup> neurons in the prelimbic area of the mPFC (PrL) was then quantified as arbitrary confocal units (a.u.) (ImageJ, NIH), and the distribution of PV immunoreactivity intensity was analyzed. PV<sup>+</sup> neurons with PV immunoreactivity intensity <2000 a.u. were classified as PV<sub>L</sub>, whereas those >2000 a.u. were classified as PV<sub>H</sub>.

### Virus injection

Stereotactic viral injections were performed in accordance with the Guidelines by Zhejiang University Animal Care and Use Committees. Mouse pups at P14 were anesthetized using isoflurane and mounted on a

stereotaxic machine. A small incision was cut to expose the skull, and two holes were drilled above the mPFC. Viral particles ( $1 \times 10^{12}$  vg/ml) were then injected at the speed of 1 nL/s through a glass micropipette using a Nanojector III (Drummond, USA) bilaterally (250 nL per injection site) into the mPFC (coordinates: A/P: +1.35 mm; M/L:  $\pm 0.2$  mm; D/V: -1.35 mm from bregma). After viral injection, wound was sutured and mice were returned to their home cages following waking up on a heating pad, and then housed under standard conditions.

### Chemogenetic manipulation

To specifically manipulating the activity of PV<sup>+</sup> neurons or glutamatergic excitatory neurons, AAVs expressing hM4Di or hM3Dq (purchased from Shanghai Taitool Bioscience) were injected into the mPFC of mice at P14, as described above. Clozapine-N-oxide (CNO) (Sigma-Aldrich, C0832) was injected once per day from P21 to P28 (5 mg/kg, i.p.), while control mice were injected with same volume of saline. CNO/saline treatment was ceased at least 3 days before behavior experiments.

### Electrophysiology

Mice were deeply anesthetized with isoflurane and decapitated rapidly. Brain was removed and 300 µm coronal slices containing the mPFC were prepared in ice-cold oxygenated artificial cerebrospinal fluid (ACSF, in mM: 126 NaCl, 3 KCl, 1 MgCl<sub>2</sub>, 2 CaCl<sub>2</sub>, 1.25 NaH<sub>2</sub>PO<sub>4</sub>, 25 NaHCO<sub>3</sub>, and 32 D-glucose) with a vibratome (Leica, VT1000s). After slicing, brain sections were incubated in ACSF at 32 °C for 15 min, and then maintained in ACSF at room temperature before recording. Slices were transferred to the recording chamber and whole-cell patch clamp recordings were performed at 32 °C.

For the assessment of connection probability between excitatory neurons, quadruple whole-cell recordings were made in adjacent mPFC pyramidal neurons. The internal solution contained (mM): 100 K-Gluconate, 20 KCl, 4 Mg-ATP, 10 Na-phosphocreatine, 0.3 GTP, 10 HEPES and 0.1% biocytin (pH 7.35, 290–300 mOsm). Direct functional synaptic connection between the recorded neurons were examined by eliciting short trains (five pulses) of precisely timed action potentials (APs) at 20 Hz in each neuron, while recording postsynaptic potentials in the rest of the recorded neurons.

For recording sEPSCs and sIPSCs in the same neuron, the internal solution contained (mM): 100 Cs-Met-sulfonate, 10 KCl, 10 K-Gluconate, 4 Mg-ATP, 10 Na-phosphocreatine, 0.3 GTP, 10 HEPES and 0.1% biocytin (pH 7.35, 290–300 mOsm). sEPSCs and sIPSCs were recorded at the holding potential of -70 mV and +10 mV, respectively.

For recording spontaneous or miniature postsynaptic currents in PV<sup>+</sup> neurons, the internal solution was the same as described above for recording spontaneous postsynaptic currents. PV<sup>+</sup> neurons were identified by their fast-spiking properties. Subsequently, sEPSCs and mEPSCs were recorded at the holding potential of -70 mV, while mIPSCs were recorded at +10 mV; mEPSCs and mIPSCs were recorded in the presence of 1 µM TTX. Slices were fixed in 4% PFA at 4 °C after recording, and then stained for biocytin and PV to confirm the identity of PV<sup>+</sup> neurons. Data from PV<sup>+</sup> cells were discarded.

All recordings were performed using an EPC10 amplifier (HEKA, Germany) with Patchmaster software (HEKA, Germany), and analyzed with Igor Pro 8.04 (Wave Metrics, USA) and Mini Analysis 6.0.3 (Synaptosoft, USA) softwares.

### High K<sup>+</sup> treatment of acute brain slices

Acute brain slices were prepared in ice-cold oxygenated ACSF as described above. Brain slices were incubated for 30 min in ACSF containing either control (3 mM) or elevated (5 mM, 10 mM) potassium ion concentrations. Slices were then maintained in control ACSF and then fixed in 4% PFA at either 2 or 4 h post incubation.

### Behavioral assays

Before behavioral experiments, mice were handled for at least 3 days and acclimatized to the designated room for 1 h. The room brightness was maintained at <50 lux. All behavioral apparatuses were wiped with 30% ethanol and dried before each trial.

1. *Open field test:* Mice were individually placed to the central zone of an open field (45 cm × 45 cm × 35 cm) and allowed to explore the apparatus freely for 10 min. Their distance traveled and time spent in the central and peripheral zones were analyzed by AnyMaze software (Stoelting, USA).

2. *Elevated plus maze*: Mice were placed in the center of an elevated plus maze with opposite open and closed arms, and allowed to freely explore the maze for 10 min. Their distance traveled and time spent in each arm were analyzed by AnyMaze software (Stoelting, USA).
3. *Three-chamber social interaction test*: The 60 cm × 40 cm × 25 cm three-chamber apparatus was divided into a 20 cm wide center chamber and two 20 cm wide side chambers. As described previously [17], the test consisted of three 10-min trials, with 10 min intertrial intervals. In trial 1, subject mice were placed in the center chamber and allowed to habituate to the apparatus by freely exploring the three chambers for 10 min, with no social stimulus mouse in either side chamber. In trial 2 (social ability test), a never-met stimulus mouse was placed under an inverted stainless-steel cup with solid bottom and bars spaced 1 cm apart, in one of the side chambers (randomly selected). In trial 3 (social novelty test), the first stimulus mouse was moved to the other side chamber, and a second never-met-before stimulus mouse was placed under another identical stainless-steel cup and put at the previous location. In trials 2 and 3, the subject mice were allowed to explore all three chambers, and their behaviors were recorded by an overhead camera. The time the subject mice spent in each chamber and the interaction time with each stimulus mouse were analyzed by AnyMaze software (Stoelting, USA). All social stimulus mice were sex-, age- and strain-matched with the subject mice, and held in a different rack.

### Statistical analysis

Data were collected double-blinded and adequate for statistical analysis using GraphPad Prism 9.4 software. Statistical analysis was carried out using two-tailed unpaired t-tests or otherwise indicated in the figure legends. Data were presented as the mean ± SEM. Statistical significance was considered when  $P < 0.05$ .

## RESULTS

### The spectrum of PV expression in the developing mPFC regulated by neuronal activity

PV<sup>+</sup> neurons, a major subpopulation of GABAergic interneurons, are widely distributed in cortical areas. To understand the developmental trajectory of PV<sup>+</sup> neurons in the mPFC of healthy brain, we profiled the spatial and temporal patterns of PV expression in the developing mPFC of wild-type C57 mice. PV immunostaining was performed after postnatal day 21 (P21) due to the late-onset of PV expression in the neocortex [18]. According to the intensity of PV immunoreactivity, we observed a broad spectrum of PV expression in mPFC PV<sup>+</sup> neurons during development (Fig. 1a, b). For instance, the distribution of PV immunoreactivity peaked at the intensity of ~1800 a.u. and ~3800 a.u. at P28 (Fig. 1b). In previous studies, similar pattern of continuous spectrum of PV expression has been observed in hippocampus [19–21]. According to the categorization employed in these studies, we then classified PV<sup>+</sup> neurons into two subpopulations based on their immunostaining intensity: high-level PV expression (PV<sub>H</sub>) neurons (intensity > 2000 a.u.) and low-level PV expression (PV<sub>L</sub>) neurons (intensity < 2000 a.u.). Both PV<sub>H</sub> and PV<sub>L</sub> neurons expressed GAD67, indicating that they were all GABAergic interneurons (Fig. 1c). In addition, we performed 3D reconstruction of PV<sub>H</sub> and PV<sub>L</sub> neurons and found both types of PV<sup>+</sup> neurons were imaged with intact cell bodies (Supplementary Fig. 1), thus excluding the possibility that low-level PV fluorescence signal was caused by non-focal imaging. The density and proportion of PV<sub>L</sub> neurons were significantly less than PV<sub>H</sub> neurons in the mPFC from P21 to P35 (Fig. 1d, e). In detail, in layer 2/3 (L2/3), PV<sub>L</sub> neurons were similar to PV<sub>H</sub> neurons at P21, and less than PV<sub>H</sub> neurons from P28 to P35, in both density and proportion (Supplementary Fig. 2a). Whereas in layer 5/6 (L5/6), the density and proportion of PV<sub>L</sub> neurons were less than PV<sub>H</sub> neurons from P21 to P35 (Supplementary Fig. 2b). These data

suggest that the distribution of PV<sub>H</sub> and PV<sub>L</sub> neurons exhibited layer-specificity along development. In contrast, nearly all PV<sup>+</sup> neurons were PV<sub>H</sub> in the primary motor cortex (M1) at the same developmental stages (Supplementary Fig. 3), indicating that the PV<sub>L</sub> subpopulation in the mPFC shows a distinct pattern compared to M1 during postnatal development.

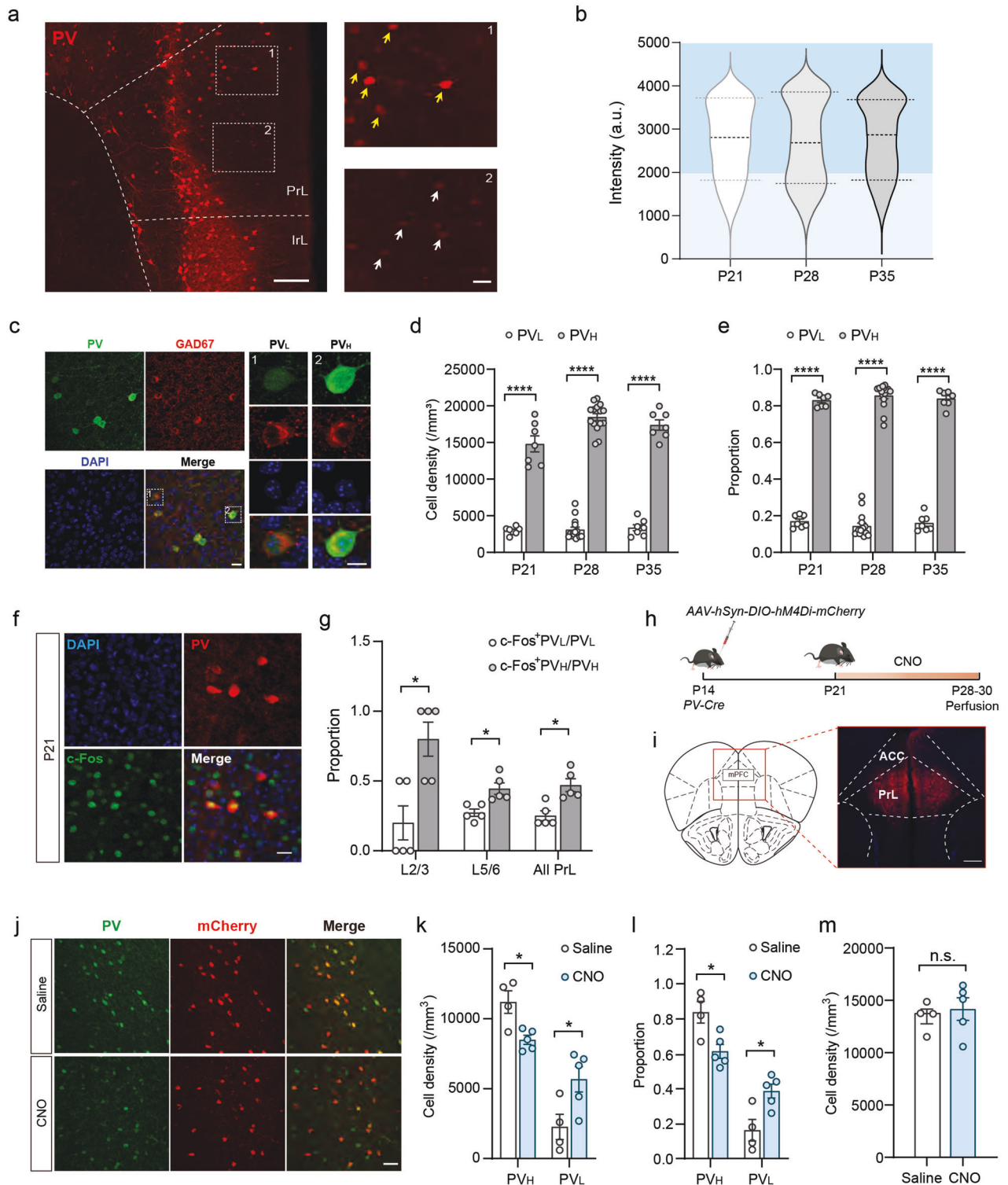
Next, we tried to identify the cause of the specific broad spectrum of PV expression in the developing mPFC. We first asked whether PV<sub>H</sub> and PV<sub>L</sub> neurons were generated at different gestation stages. We injected BrdU intraperitoneally at embryonic day 11.5 (E11.5), 13.5 (E13.5) or 15.5 (E15.5) to label neurons born at different stages. Dual-staining of BrdU and PV showed that the proportion of PV<sub>L</sub> neurons born at E11.5, E13.5, or E15.5 was similar to that of PV<sub>H</sub> neurons in the mPFC at P21 (Supplementary Fig. 4a, b). These data suggest that mPFC PV<sub>H</sub> and PV<sub>L</sub> neurons are generated from the same cell lineage so that the expression of PV is independent of the age of PV<sup>+</sup> neurons in the mPFC.

We then tested the possibility that the expression of PV may be related to the maturity of PV<sup>+</sup> neurons. Previous studies have reported that matured PV<sup>+</sup> neurons tend to be enwrapped by perinatal nets (PNNs), a specialized extracellular matrix structure that can be indicated by wisteria floribunda agglutinin (WFA), a specific marker of PNNs [22]. Thus, we performed double immunostaining of WFA and PV in the mPFC sections from P28 to P42 (Supplementary Fig. 4c). No significant difference was found in the co-labeling of WFA surrounding PV<sub>H</sub> or PV<sub>L</sub> neurons in the mPFC at either P28 or P42 (Supplementary Fig. 4d), suggesting that PV expression level is not related to the maturity of PV<sup>+</sup> neurons in the developing mPFC. Different from the relatively sparse WFA signals in the mPFC, WFA in M1 were much stronger at the same developmental stages (Supplementary Fig. 5a, b). The co-labeling of WFA and PV in M1 was also considerably higher than in the mPFC (Supplementary Fig. 5a, c). These results strongly indicate that the maturation of PV<sup>+</sup> neurons in the mPFC is significantly delayed in comparison to that in M1.

Finally, we tested the possibility that the level of PV expression is regulated by the activity of these PV<sup>+</sup> neurons in the developing mPFC. Dual-staining of c-Fos and PV showed higher rate of colocalization of c-Fos with PV<sub>H</sub> neurons than that with PV<sub>L</sub> neurons in both L2/3 and L5/6 (Fig. 1f, g), implying PV expression might be related to the activity of PV<sup>+</sup> neurons. To test this assumption, we incubated acute brain slices in ACSF with high potassium concentration (5 mM or 10 mM). We found the proportion of PV<sub>L</sub> neurons was significantly decreased while that of PV<sub>H</sub> neurons increased by high potassium treatment (Supplementary Fig. 6a, b). To further confirm this *in vivo*, we injected AAV-hSyn-DIO-hM4Di-mCherry into the mPFC of PV-Cre mice at P14 and applied CNO from P21 to P28 to specifically decrease the activity of mPFC PV<sup>+</sup> neurons (Fig. 1h, i). Indeed, both the density and proportion of PV<sub>H</sub> neurons decreased, while those of PV<sub>L</sub> neurons increased at P28 (Fig. 1j–l). Moreover, we found no difference in the density of mCherry<sup>+</sup> neurons in the mPFC between CNO and saline-treated mice (Fig. 1m), indicating that the number of total PV<sup>+</sup> neurons was not altered in CNO group. These results suggest that PV expression is determined by the activity of individual PV<sup>+</sup> neurons in the mPFC. Therefore, the broad spectrum of PV expression reflects various activity states of PV<sup>+</sup> interneurons in the mPFC during postnatal development.

### PV<sub>H</sub>-to-PV<sub>L</sub> transition in the developing mPFC of VPA mice

It has been well known that valproic acid (VPA) exposure during pregnancy leads to high risk of autism in children [23]. Therefore, gestational VPA exposure has been developed to a reliable ASD animal model in rodents and non-human primates [24, 25]. Here, we prepared VPA-exposed mice (VPA mice) by injecting VPA at E12.5, while control mice were prepared by injecting the same volume of saline at the same gestation time (Ctrl) (Fig. 2a). We found that VPA mice exhibited normal social ability compared to



Ctrl mice (Supplementary Fig. 7a). However, these mice did not show a significant preference to interact with a stranger mouse in the three-chamber social novelty task (Fig. 2b–d), indicating a social novelty deficit, which represents a classic social behavior abnormality in ASD and is consistent with previous studies [26]. The performance of VPA mice in both open field (OF) and elevated plus maze (EPM) tests was similar to that of Ctrl mice (Supplementary Fig. 7b, c), suggesting that VPA mice have a normal anxiety level.

Interestingly, at P21, both the density and proportion of PV<sub>L</sub> neurons increased significantly, while that of PV<sub>H</sub> neurons decreased significantly (Fig. 2e–g) in the mPFC of VPA mice compared to Ctrl mice, as shown by a downward shift in the spectrum of PV expression (Fig. 2h). We observed similar results at P28 (Fig. 2i–l). Further analysis revealed that the density of total PV<sup>+</sup> neurons in the mPFC was unaltered at P21 (Fig. 2m) and slightly reduced at P28 (Fig. 2n) in VPA mice. These data indicated a significant PV<sub>H</sub>-to-PV<sub>L</sub> transition in the developing mPFC of VPA mice.

**Fig. 1 The spectrum of PV expression in the developing mPFC regulated by neuronal activity.** **a** Left: A representative image showing PV immunoreactivity in the mPFC at P21. Scale bar, 200  $\mu\text{m}$ . Right: Zoom-in images showing PV<sub>H</sub> (yellow arrows) and PV<sub>L</sub> (white arrows) neurons in selected regions (dashed boxes) in the left panel. Scale bar, 20  $\mu\text{m}$ . **b** The distribution of PV immunoreactivity intensity (a.u.) in the mPFC at P21, P28 and P35. **c** Left: Images showing both PV<sub>H</sub> and PV<sub>L</sub> neurons expressed GAD67. Scale bar, 20  $\mu\text{m}$ . Right: Representative PV<sub>H</sub> and PV<sub>L</sub> neurons in the dashed boxes in the left. Scale bar, 10  $\mu\text{m}$ . **d** The density of PV<sub>H</sub> and PV<sub>L</sub> neurons in the mPFC at P21, P28 and P35 (P21: n = 7 mice, paired t test,  $t = 10.84$ ,  $df = 6$ , \*\*\*\* $P < 0.0001$ ; P28: n = 15 mice, paired t test,  $t = 19.55$ ,  $df = 14$ , \*\*\*\* $P < 0.0001$ ; P35: n = 7 mice, paired t test,  $t = 18.56$ ,  $df = 6$ , \*\*\*\* $P < 0.0001$ ). **e** The proportion of PV<sub>H</sub> and PV<sub>L</sub> neurons in the mPFC at P21, P28 and P35 (P21: n = 7 mice, paired t test,  $t = 25.41$ ,  $df = 6$ , \*\*\*\* $P < 0.0001$ ; P28: n = 15 mice, paired t test,  $t = 21.24$ ,  $df = 14$ , \*\*\*\* $P < 0.0001$ ; P35: n = 7 mice, paired t test,  $t = 19.99$ ,  $df = 6$ , \*\*\*\* $P < 0.0001$ ). **f** Representative images showing double-staining of c-Fos (green) and PV (red) in the mPFC at P21. Scale bar, 20  $\mu\text{m}$ . **g** The colocalization of c-Fos with PV<sub>H</sub> neurons is higher than that with PV<sub>L</sub> neurons in both L2/3 and L5/6 (L2/3: n = 5 mice, paired t test,  $t = 3.207$ ,  $df = 4$ , \* $P = 0.0327$ ; L5/6: n = 5 mice, paired t test,  $t = 2.788$ ,  $df = 4$ , \* $P = 0.0494$ ; All PrL: n = 5 mice, paired t test,  $t = 3.333$ ,  $df = 4$ , \* $P = 0.029$ ). **h** Schematics showing the chemogenetic approach to down-regulate the activity of PV<sup>+</sup> neurons in the mPFC. **i** Representative image showing the site of virus injection in the mPFC. Scale bar, 500  $\mu\text{m}$ . **j** Representative images showing PV expression (green) in PV<sup>+</sup> neurons (mCherry) in the mPFC of saline- and CNO-treated mice. Scale bar, 50  $\mu\text{m}$ . **k** The density of PV<sub>H</sub> neurons decreased while the density of PV<sub>L</sub> neurons increased in the mPFC of CNO-treated mice (PV<sub>H</sub>: saline n = 4 mice, CNO n = 5 mice,  $t = 3.41$ ,  $df = 7$ , \* $P = 0.0113$ ; PV<sub>L</sub>: saline n = 4 mice, CNO n = 5 mice,  $t = 2.62$ ,  $df = 7$ , \* $P = 0.0345$ ). **l** The proportion of PV<sub>H</sub> neurons decreased while the proportion of PV<sub>L</sub> neurons increased in the mPFC of CNO-treated mice (PV<sub>H</sub>: saline n = 4 mice, CNO n = 5 mice,  $t = 3.15$ ,  $df = 7$ , \* $P = 0.0161$ ; PV<sub>L</sub>: saline n = 4 mice, CNO n = 5 mice,  $t = 3.15$ ,  $df = 7$ , \* $P = 0.0161$ ). **m** There was no significant difference between the density of total PV<sup>+</sup> neurons in the mPFC of saline- and CNO-treated mice (saline: n = 4 mice, CNO: n = 5 mice,  $t = 0.52$ ,  $df = 7$ ,  $P = 0.6212$ ). Data are represented as mean  $\pm$  SEM.

Since the expression of PV in individual PV<sup>+</sup> neurons during mPFC development is regulated by their activity, we then tested whether this PV<sub>H</sub>-to-PV<sub>L</sub> transition in the mPFC of VPA mice was caused by decreased activity of these neurons. Indeed, in the mPFC of VPA mice at P21, we observed a reduced colocalization of c-Fos and PV<sup>+</sup> neurons, compared to Ctrl mice of the same age (Fig. 2o, p), suggesting a generally decreased activity of PV<sup>+</sup> neurons in the developing mPFC of VPA mice. Together, these results indicated that the PV<sub>H</sub>-to-PV<sub>L</sub> transition in the mPFC of VPA mice was related to the decreased activity of these PV<sup>+</sup> neurons.

#### Decreased activity of excitatory neurons reduced excitatory drive to PV<sup>+</sup> neurons

To further investigate possible mechanisms underlying the decreased activity of PV<sup>+</sup> neurons in the developing mPFC of VPA mice, we conducted whole-cell recordings on mPFC PV<sup>+</sup> neurons in acute brain slices at P21 (Fig. 3a). Our results showed that the intrinsic firing property of PV<sup>+</sup> neurons in the mPFC was not altered in VPA mice (Supplementary Fig. 8a–f).

Cortical PV<sup>+</sup> neurons are known to receive intense inputs from neighboring excitatory pyramidal neurons as well as project to them. Therefore, we examined the synaptic inputs to PV<sup>+</sup> neurons in the mPFC by recording spontaneous postsynaptic currents. Although the amplitude of spontaneous excitatory postsynaptic currents (sEPSCs) recorded from PV<sup>+</sup> neurons showed a tendency to increase, the frequency of sEPSCs was significantly reduced in VPA mice, leading to a decrease in the total excitatory charge received by PV<sup>+</sup> neurons per unit time (Fig. 3b–e).

To validate whether there are any changes in synaptic sites on PV<sup>+</sup> neurons, we next recorded miniature postsynaptic currents in mPFC PV<sup>+</sup> neurons in control and VPA mice at P21. We found that the frequency of miniature excitatory postsynaptic currents (mEPSCs) was significantly decreased in mPFC PV<sup>+</sup> neurons in VPA mice, without a significant change in the amplitude, resulting in significantly decreased excitatory charge (Supplementary Fig. 8g–j). Whereas, the frequency of miniature inhibitory postsynaptic currents (mIPSCs) was not altered in mPFC PV<sup>+</sup> neurons in VPA mice (Supplementary Fig. 8k, l). Although the average amplitude of mIPSCs was increased, the total inhibitory charge remained unchanged in mPFC PV<sup>+</sup> neurons in VPA mice (Supplementary Fig. 8m, n). We further analyzed the dendritic spines in labeled mPFC PV<sup>+</sup> neurons and found that PV<sup>+</sup> neurons in VPA mice exhibited significantly decreased spine density, compared to control mice (Supplementary Fig. 8o, p). These data suggest that the excitatory synaptic sites were significantly reduced in mPFC PV<sup>+</sup> neurons in VPA mice.

To examine whether changes in the activity of surrounding pyramidal neurons also contribute to the reduced excitatory drive

to mPFC PV<sup>+</sup> neurons in VPA mice, we then quantified colocalization of c-Fos and CaMKII<sup>+</sup> neurons. We found a dramatic decrease in the density of c-Fos<sup>+</sup>CaMKII<sup>+</sup> neurons in the mPFC of VPA mice at P21 (Fig. 3f, g), indicating a substantial reduction in the activity of mPFC excitatory microcircuits in VPA mice.

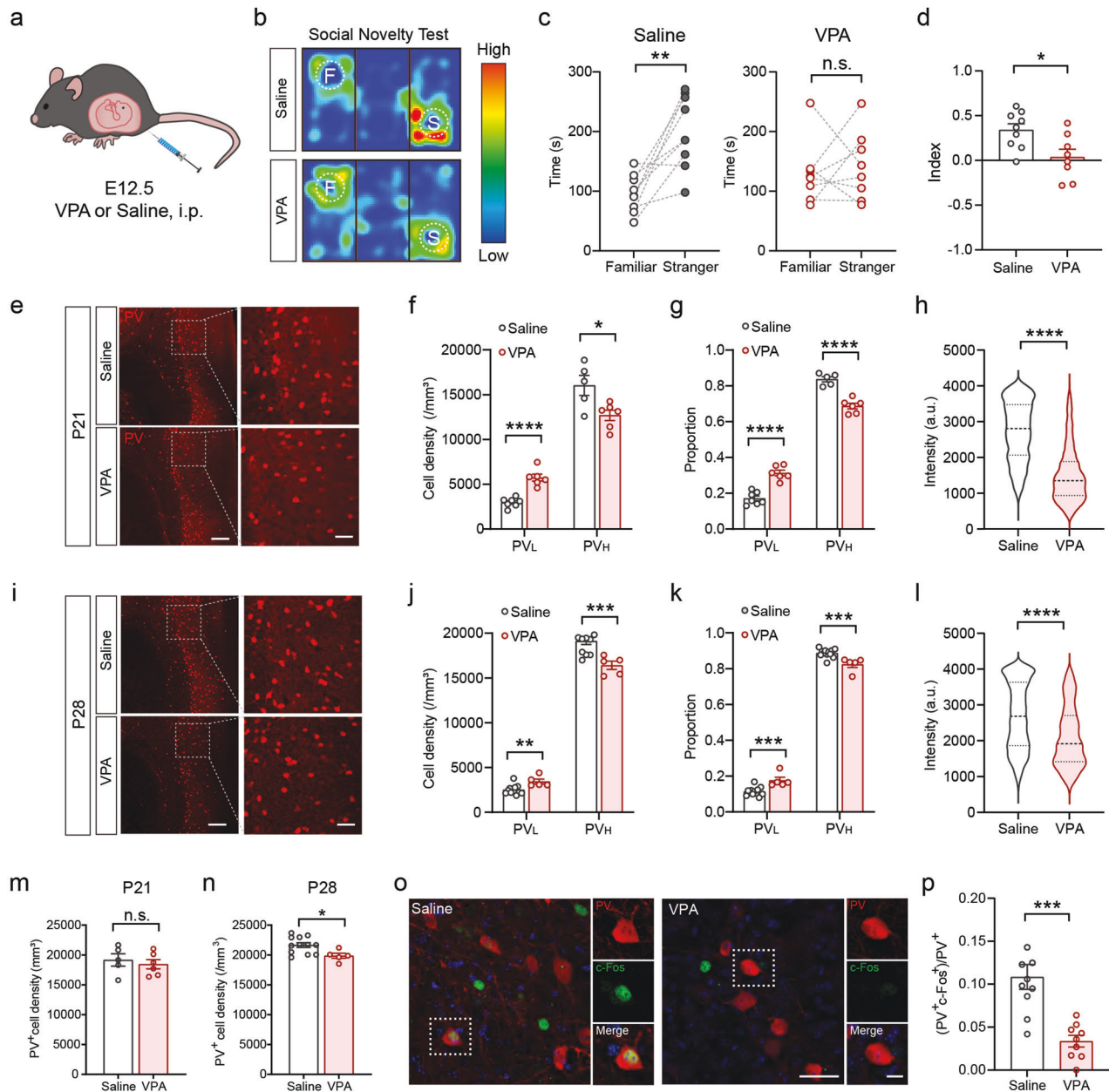
To evaluate the activity of excitatory microcircuits in the developing mPFC, we then performed quadruple whole-cell recordings in acute brain slices (Fig. 3h). Our results showed that the connection probability between mPFC pyramidal neurons was significantly lower in VPA mice at P14 and P21 (Fig. 3i), indicating weakened communication within local excitatory networks in the mPFC of VPA mice. Furthermore, we observed a significantly decreased frequency of sEPSCs recorded from mPFC pyramidal neurons in VPA mice without a change in amplitude at P21 and P28, leading to a decreased total excitatory charge from P21 (Fig. 3j–m). These findings suggested a decreased activity of excitatory microcircuits in the developing mPFC of VPA mice.

Interestingly, we found that the amplitude but not frequency of spontaneous inhibitory postsynaptic currents (sIPSCs) of mPFC pyramidal neurons decreased in VPA mice. As a result, there was a decrease in the total inhibitory charge from P28 (Fig. 3n–q), suggesting a delayed onset of reduced activity of inhibitory microcircuits in the mPFC of VPA mice. These results indicate that the reduction in excitatory activity occurred 1 week earlier than the reduction in inhibitory activity in the developing mPFC of VPA mice.

In addition, since both excitatory and inhibitory activities were reduced in the mPFC of VPA mice, we investigated whether the E/I ratio in the mPFC was altered in these mice. By measuring the total charge of both sEPSCs and sIPSCs per unit time in pyramidal neurons, we found that the E/I ratio in the mPFC of VPA mice did not change significantly from P21 to P35, compared to Ctrl mice (Supplementary Fig. 9a–c). In addition, we also recorded electrically-evoked postsynaptic currents in mPFC pyramidal neurons at P21. Although the evoked excitatory postsynaptic currents (eEPSCs) and evoked inhibitory postsynaptic currents (eIPSCs) both decreased in VPA mice (Supplementary Fig. 9d, e), the E/I ratio remained at a similar level compared to control mice (Supplementary Fig. 9f, g). These results suggest that the E/I ratio of basal synaptic transmission during postnatal development may not be necessarily altered for inducing cortical circuit dysfunction in ASD.

#### Decreased excitation but not PV<sup>+</sup> interneuron-mediated inhibition in the developing mPFC reproduced ASD-like social novelty deficit

To verify that the decreased excitatory activity further mediated the PV<sub>H</sub>-to-PV<sub>L</sub> transition in the mPFC of VPA mice, we co-injected



AAV-CaMKII $\alpha$ -hM4Di-mCherry and AAV-hSyn-DIO-GFP into the mPFC of PV-Cre mice at P14 and applied CNO from P21 to P28 to selectively suppress the activity of mPFC excitatory microcircuits within a narrow window (Fig. 4a, b). Our results showed that the density and proportion of PV<sub>L</sub> neurons were increased, accompanied by a decrease in the density and proportion of PV<sub>H</sub> neurons (Fig. 4c–e), indicating a PV<sub>H</sub>-to-PV<sub>L</sub> transition induced by decreased excitation in the mPFC. However, the density of GFP<sup>+</sup> neurons was not altered (Fig. 4f), suggesting that the total number of PV<sup>+</sup> neurons was not affected. These results are consistent with the PV<sub>H</sub>-to-PV<sub>L</sub> transition observed in the developing mPFC of VPA mice.

In addition, selectively suppressing the activity of excitatory pyramidal neurons from P21 to P28 induced severe social novelty deficit in these animals at P28–30 (Fig. 4g–j), resembling the behavioral phenotype of VPA mice. There were no significant differences in social ability or anxiety levels between the mice treated with CNO or saline (Supplementary Fig. 10a–c). These results indicate that reduced excitatory activity in the mPFC during

postnatal development not only leads to a PV<sub>H</sub>-to-PV<sub>L</sub> transition but also replicates ASD-like social novelty deficit in adolescence.

Since suppressing PV<sup>+</sup> interneuron-mediated inhibitory activity also led to a PV<sub>H</sub>-to-PV<sub>L</sub> transition in the developing mPFC as shown in Fig. 1h–m, we then examined whether suppressing the activity of PV<sup>+</sup> neurons in the mPFC could induce ASD-like social deficits. We injected AAV-hSyn-DIO-hM4Di-mCherry into the mPFC of PV-Cre mice at P14 and continuously administered CNO from P21 to P28 to mimic the decreased activity of PV<sup>+</sup> neurons in VPA mice during postnatal development (Fig. 4k). Surprisingly, we did not observe either impaired social novelty (Fig. 4l–n) or abnormal social ability in these mice (Supplementary Fig. 11d), compared to Ctrl mice which were injected with the same virus but treated with saline. The performance of the mice in OF or EPM tests was not affected (Supplementary Fig. 11e, f), reflecting their normal anxiety level. These findings suggest that although the reduction in the activity of PV<sup>+</sup> neurons leads to a PV<sub>H</sub>-to-PV<sub>L</sub> transition in the developing mPFC, it may not be the primary driver of ASD-like social cognitive deficits.

**Fig. 2** **PV<sub>H</sub>-to-PV<sub>L</sub> transition in the developing mPFC of VPA mice.** **a** Schematics showing the preparation of VPA or Saline (control) mice by i.p. injection of VPA or saline at E12.5. **b** Position heat map of Saline (top) and VPA (bottom) mice in social novelty test. **c** The time that Saline or VPA mice spent on the interaction with familiar and stranger mice (Saline:  $n = 9$  mice, paired  $t$  test,  $t = 4.52$ ,  $df = 8$ ,  $**P = 0.0020$ ; VPA:  $n = 8$  mice, paired  $t$  test,  $t = 0.46$ ,  $df = 7$ ,  $P = 0.6617$ ). **d** Social discrimination index of Saline and VPA mice in the social novelty test (Saline:  $n = 9$  mice, VPA:  $n = 8$  mice,  $t = 2.76$ ,  $df = 15$ ,  $*P = 0.0147$ ). **e** Representative images showing PV immunoreactivity in the mPFC of Saline and VPA mice at P21. Scale bars, 200  $\mu\text{m}$  or 50  $\mu\text{m}$  (in zoom-in images). **f** The density of PV<sub>H</sub> neurons decreased while the density of PV<sub>L</sub> neurons increased in the mPFC of VPA mice at P21 (PV<sub>L</sub>: Saline  $n = 7$  mice, VPA  $n = 6$  mice,  $t = 6.63$ ,  $df = 11$ ,  $****P < 0.0001$ ; PV<sub>H</sub>: Saline  $n = 5$  mice, VPA  $n = 6$  mice,  $t = 2.81$ ,  $df = 9$ ,  $*P = 0.0205$ ). **g** The proportion of PV<sub>H</sub> neurons decreased while the proportion of PV<sub>L</sub> neurons increased in the mPFC of VPA mice at P21 (PV<sub>L</sub>: Saline  $n = 7$  mice, VPA  $n = 6$  mice,  $t = 6.84$ ,  $df = 11$ ,  $****P < 0.0001$ ; PV<sub>H</sub>: Saline  $n = 5$  mice, VPA  $n = 6$  mice,  $t = 6.72$ ,  $df = 9$ ,  $****P < 0.0001$ ). **h** The distribution of PV immunoreactivity intensity in the mPFC of Saline and VPA mice at P21 (Saline:  $N = 5$  mice,  $n = 1932$  cells, VPA:  $N = 4$  mice,  $n = 1599$  cells,  $t = 44.85$ ,  $df = 3529$ ,  $****P < 0.0001$ ). **i** Representative images showing PV immunoreactivity in the mPFC of Saline and VPA mice at P28. Scale bar, 200  $\mu\text{m}$  or 50  $\mu\text{m}$  (in zoom-in images). **j** The density of PV<sub>H</sub> neurons decreased while the density of PV<sub>L</sub> neurons increased in the mPFC of VPA mice at P28 (PV<sub>L</sub>: Saline  $n = 12$  mice, VPA  $n = 5$  mice,  $t = 3.33$ ,  $df = 15$ ,  $**P = 0.0046$ ; PV<sub>H</sub>: Saline  $n = 12$  mice, VPA  $n = 5$  mice,  $t = 4.09$ ,  $df = 15$ ,  $***P = 0.001$ ). **k** The proportion of PV<sub>H</sub> neurons decreased while the proportion of PV<sub>L</sub> neurons increased in the mPFC of VPA mice at P28 (PV<sub>L</sub>: Saline  $n = 12$  mice, VPA  $n = 5$  mice,  $t = 4.14$ ,  $df = 15$ ,  $***P = 0.0009$ ; PV<sub>H</sub>: Saline  $n = 12$  mice, VPA  $n = 5$  mice,  $t = 4.14$ ,  $df = 15$ ,  $***P = 0.0009$ ). **l** The distribution of PV immunoreactivity intensity in the mPFC of Saline and VPA mice at P28 (Saline:  $N = 5$  mice,  $n = 1992$  cells, VPA:  $N = 3$  mice,  $n = 1230$  cells,  $t = 18.25$ ,  $df = 3220$ ,  $****P < 0.0001$ ). **m** The density of total PV<sup>+</sup> neurons in the mPFC of Saline and VPA mice at P21 (Saline:  $n = 5$  mice,  $n = 6$  mice,  $t = 0.56$ ,  $df = 9$ ,  $P = 0.5872$ ). **n** The density of total PV<sup>+</sup> neurons in the mPFC of Saline and VPA mice at P28 (Saline:  $n = 12$  mice, VPA:  $n = 5$  mice,  $t = 2.61$ ,  $df = 15$ ,  $*P = 0.0199$ ). **o** Representative images showing the colocalization of c-Fos (green) and PV<sup>+</sup> neurons (red) in the mPFC of Saline (left) and VPA (right) mice at P21. Scale bars, 25  $\mu\text{m}$  or 5  $\mu\text{m}$  (in zoom-in images). **p** The proportion of c-Fos<sup>+</sup>PV<sup>+</sup> neurons in all PV<sup>+</sup> neurons in the mPFC of Saline and VPA mice at P21 (Saline:  $n = 10$  mice, VPA:  $n = 9$  mice,  $t = 4.48$ ,  $df = 17$ ,  $***P = 0.0003$ ). Data are represented as mean  $\pm$  SEM.

### Enhancing excitation but not PV<sup>+</sup> interneuron-mediated inhibition in the developing mPFC rescued social deficit in VPA mice

After identifying the dominant role of mPFC excitatory activity in mediating ASD-like social cognitive deficits, we sought to investigate whether enhancing excitatory activity in the developing mPFC could prevent the reduction in the activity of PV<sup>+</sup> neurons in VPA mice and rescue their social novelty deficit. To address this question, we injected AAV-CaMKII $\alpha$ -hM3Dq-mCherry into the mPFC of VPA mice at P14 and continuously administered CNO from P21 to P28 to selectively enhance excitatory activity in the mPFC within a specific time window (Fig. 5a, b). We found the proportion of PV<sub>L</sub> neurons were decreased at P28, while that of PV<sub>H</sub> neurons were increased (Fig. 5c, d), compared to control VPA mice that were injected with the same combination of viruses but treated with saline. This result suggests that enhanced excitation did prevent the PV<sub>H</sub>-to-PV<sub>L</sub> transition in VPA mice. Moreover, increasing the activity of excitatory neurons in the mPFC during this time window successfully rescued social novelty deficit in VPA mice (Fig. 5e–g). The social ability or anxiety level of VPA mice was not affected by CNO treatment (Supplementary Fig. 12a–c). For comparison, we also injected AAV expressing hM3Dq driven by parvalbumin promoter (AAV-PV.S5E2-hM3Dq-mCherry) into the mPFC of VPA mice to selectively enhance PV<sup>+</sup> interneuron activity during postnatal development (Fig. 5h). Our results showed that increasing PV<sup>+</sup> interneuron-mediated inhibition did not rescue social novelty deficit in VPA mice (Fig. 5i–k). In addition, we examined the virally-labeled neurons in the mPFC after behavioral tests (Fig. 5l). Consistent with previous research [27], our immunostaining showed that the majority of the mCherry<sup>+</sup> neurons were PV<sup>+</sup> (Fig. 5m), suggesting a specific targeting of PV<sup>+</sup> interneuron by the virus. CNO treatment significantly increased the colocalization of c-Fos and mCherry<sup>+</sup> neurons (Fig. 5n), confirming an enhanced activity of mCherry<sup>+</sup> neurons by pharmacogenetic activation. Taken together, our results indicate that enhancing the activity of mPFC excitatory microcircuits within a key developmental time window could prevent the down-regulated activity of PV<sup>+</sup> neurons in VPA mice and lead to the recovery of their social functions.

### Enhancing excitation in the developing mPFC rescued social deficit in FMR1 KO mice

We also investigated the causal relationship between excitatory activity, PV<sup>+</sup> interneurons, and impaired social functions in FMR1 KO mice, a well-established transgenic animal model for Fragile X

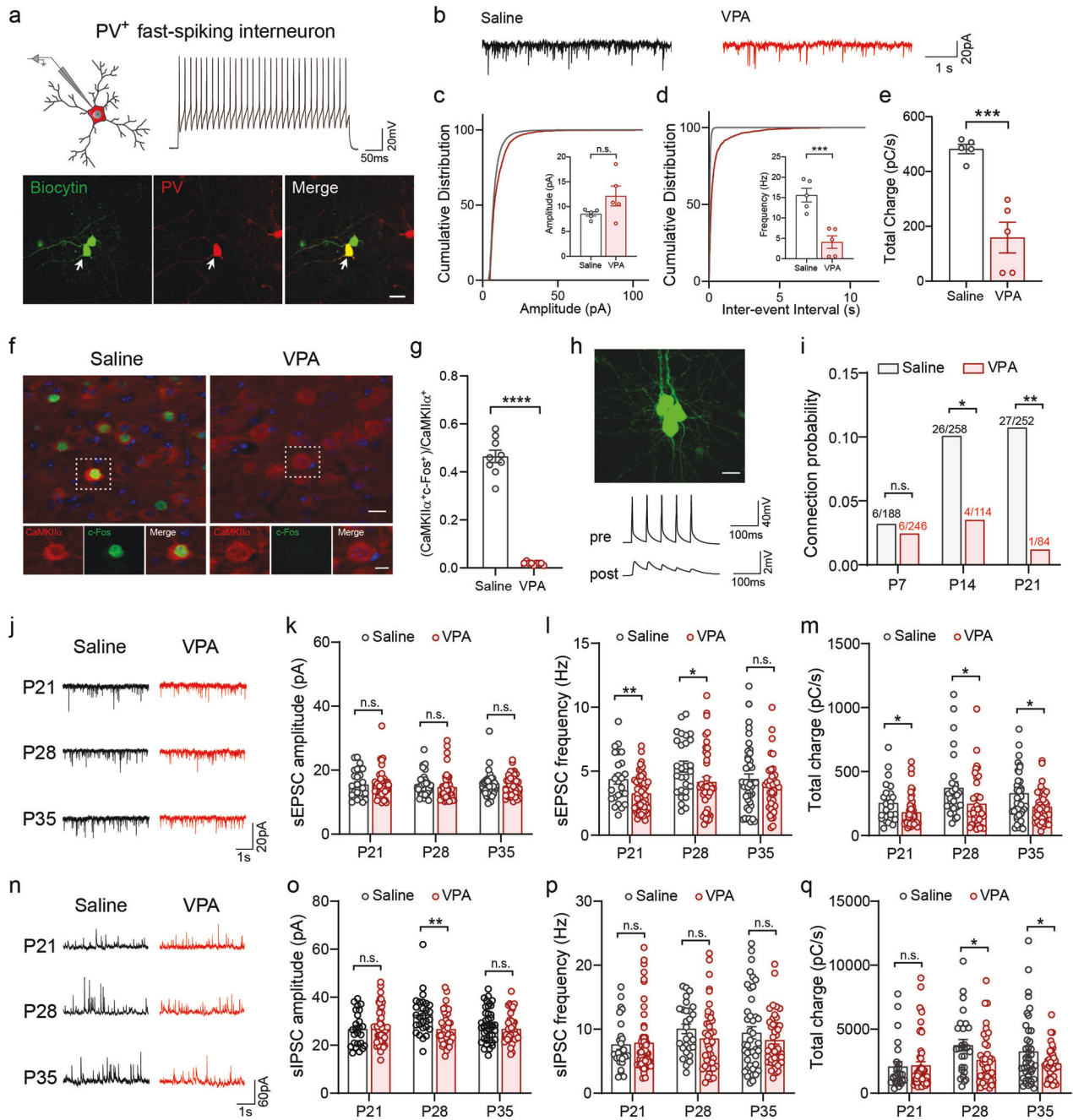
Syndrome with severe social cognitive deficits [28]. Our results confirmed that FMR1 KO mice (KO) exhibited normal social ability (Supplementary Fig. 13a), but spent less time interacting with the stranger mouse (Fig. 6a–c), compared to wild-type mice (WT) of the same age. Furthermore, these FMR1 KO mice spent more time in the center zone during the OF test (Supplementary Fig. 13b) and a similar amount of time in the open arms during the EPM test (Supplementary Fig. 13c), compared to WT mice. These findings suggest that FMR1 KO mice displayed decreased anxiety-like behavior and typical social novelty deficits, consistent with previous studies [28, 29].

We next examined the alterations in PV<sup>+</sup> neurons in the mPFC of FMR1 KO mice at P21. Compared to WT mice, FMR1 KO mice showed decreased PV<sub>H</sub> neurons and increased PV<sub>L</sub> neurons in the mPFC (Fig. 6d, e), which was consistent with what we have observed in VPA mice. This suggests that the activity state of PV<sup>+</sup> neurons in the mPFC of FMR1 KO mice was similarly down-regulated during postnatal development. Then we selectively increased the activity of excitatory neurons by injecting AAV-CaMKII $\alpha$ -hM3Dq-mCherry into the mPFC of FMR1 KO mice at P14 and continuously applying CNO or saline from P21 to P28 (Fig. 6f, g). We found that enhancing the excitatory activity restored the proportion of PV<sub>H</sub> and PV<sub>L</sub> neurons in the mPFC of FMR1 KO mice treated with CNO (Fig. 6h, i). More importantly, CNO-treated FMR1 KO mice exhibited normal social ability (Supplementary Fig. 13d) and greatly improved social novelty recognition (Fig. 6j–l). In addition, enhancing the excitatory activity slightly reduced the time that FMR1 KO mice spent in the center zone during the OF test (Supplementary Fig. 13e), and did not alter the performance of these mice in the EPM test (Supplementary Fig. 13f). Taken together, these findings suggest that reduced excitatory activity in the developing mPFC could be a common local circuit mechanism for the down-regulated activity of PV<sup>+</sup> neurons and impaired social functions in different ASD animal models.

## DISCUSSION

### PV<sub>H</sub> and PV<sub>L</sub> subpopulations in the developing mPFC

While previous studies primarily focused on those neurons characterized by high-level PV expressions and often overlooked the neurons characterized by low-level PV expression, our study discovered a continuous spectrum of PV expression in the mPFC and aimed to conduct a comprehensive analysis of the entire PV neuron population. Based on PV immunostaining intensity, we classified PV<sup>+</sup> interneurons into PV<sub>H</sub> and PV<sub>L</sub> subpopulations, similar to what has been reported in the hippocampus [19].



However, our study has several distinctive findings that are noteworthy. Firstly, by using cell lineage tracing experiments, we found the majority of both PV<sub>H</sub> and PV<sub>L</sub> neurons in the mPFC were born at E11.5, which is within the typical time window for the generation of cortical PV<sup>+</sup> neurons [30]. This suggests that PV<sub>H</sub> and PV<sub>L</sub> neurons in the mPFC are generated at the same developmental stages and are likely derived from the same cell lineage. This is different from the hippocampal PV<sub>H</sub> and PV<sub>L</sub> neurons reported in previous studies, which are generated at different embryonic stages and are therefore likely to be derived from different cell lineages [20]. Secondly, we observed PV<sub>H</sub> and PV<sub>L</sub> neurons specifically in the mPFC but not in M1 during postnatal development, and we found lower level of PNNs in the mPFC than in M1, indicating that the mPFC is less mature than M1 at the same age. These findings suggest that the specific PV<sub>H</sub>/PV<sub>L</sub> pattern may be an important indicator of a prolonged maturation

of mPFC during postnatal development. Finally, we found that the expression level of PV is closely correlated to the activity of PV<sup>+</sup> neurons and that there is a PV<sub>H</sub>-to-PV<sub>L</sub> transition in both VPA and FMR1 KO mice. Although there might be variations in the PV<sub>H</sub>-to-PV<sub>L</sub> ratio in different layers or in different animals using consistent criteria, we observed similar changes in PV<sub>H</sub> and PV<sub>L</sub> subpopulations in the mPFC in both VPA and FMR1 KO mice. Therefore, the mPFC-specific PV<sub>H</sub>-to-PV<sub>L</sub> transition could be a shared feature indicating abnormal circuit activity in neurodevelopmental disorders such as ASD.

#### Decreased PV expression but not less PV<sup>+</sup> neurons in ASD

The density of neurons exhibiting PV-immunoreactivity has been observed to be decreased in multiple ASD animal models, but there has been long-standing controversy over whether the number of PV<sup>+</sup> neurons is reduced or if the expression of PV



**Fig. 3** **Decreased activity of excitatory neurons reduced excitatory drive to PV<sup>+</sup> neurons.** **a** Top: Whole-cell patch recording and typical fast-spiking firing pattern of PV<sup>+</sup> neurons; Bottom: post-hoc staining of recorded PV<sup>+</sup> neuron (white arrow). Scale bar, 20  $\mu$ m. **b** Representative traces of sEPSCs recorded from PV<sup>+</sup> neurons in the mPFC of Saline and VPA mice at P21. **c** Cumulative distribution of the amplitude of sEPSCs recorded from PV<sup>+</sup> neurons in the mPFC of Saline and VPA mice (Saline: n = 5 cells, VPA: n = 5 cells, K-S test, \*\*\*\*P < 0.0001). Inset: The average amplitude of sEPSCs (Saline: n = 5 cells, VPA: n = 5 cells, t = 1.77, df = 8, P = 0.1156). **d** Cumulative distribution of the inter-event intervals of sEPSCs recorded from PV<sup>+</sup> neurons in the mPFC of Saline and VPA mice (Saline: n = 5 cells, VPA: n = 5 cells, K-S test, \*\*\*\*P < 0.0001). Inset: The average frequency of sEPSCs (Saline: n = 5 cells, VPA: n = 5 cells, t = 5.08, df = 8, \*\*\*P = 0.001). **e** The total charge of sEPSCs per second recorded from PV<sup>+</sup> neurons in the mPFC of Saline and VPA mice (Saline: n = 5 cells, VPA: n = 5 cells, t = 5.53, df = 8, \*\*\*P = 0.0006). **f** Representative images showing the colocalization of c-Fos (green) and CaMKII (red) in Saline (left) and VPA (right) mice at P21. Scale bar, 20  $\mu$ m. Bottom row shows the Zoom-in images of the selected cells in the dashed boxes. Scale bar, 10  $\mu$ m. **g** The proportion of c-Fos<sup>+</sup> CaMKII<sup>+</sup> neurons in CaMKII<sup>+</sup> neurons in the mPFC of Saline and VPA mice at P21 (Saline: n = 9 mice, VPA: n = 9 mice, t = 17.24, df = 16, \*\*\*\*P < 0.0001). **h** Top: A representative image showing quadruple whole-cell recording in the mPFC slice at P21. Scale bar, 20  $\mu$ m. Bottom: Representative traces showing functional synaptic connection between adjacent pyramidal neurons. **i** The connection probability between pyramidal neurons in the mPFC of Saline and VPA mice at P7, P14 and P21 (P7: Saline n = 6 connected pairs from 188 tested pairs, VPA n = 6 connected pairs from 246 tested pairs, Chi-square test, P = 0.645; P14: n = 26 connected pairs from 258 tested pairs, VPA n = 4 connected pairs from 114 tested pairs, Chi-square test, \*P = 0.045; P21: Saline n = 27 connected pairs from 252 tested pairs, VPA n = 1 connected pair from 84 tested pairs, Chi-square test, \*\*P = 0.01). **j** Representative traces showing sEPSCs recorded from pyramidal neurons in the mPFC of Saline and VPA mice at P21, P28, and P35. **k** The average amplitude of sEPSCs recorded from pyramidal neurons in the mPFC of Saline and VPA mice at P21, P28 and P35 (P21: Saline n = 25 cells, VPA n = 54 cells, t = 0.39, df = 77, P = 0.6965; P28: Saline n = 28 cells, VPA n = 42 cells, t = 0.85, df = 68, P = 0.3983; P35: Saline n = 42 cells, VPA n = 41 cells, t = 0.39, df = 81, P = 0.6964). **l** The average frequency of sEPSCs recorded from pyramidal neurons in the mPFC of Saline and VPA mice at P21, P28 and P35 (P21: Saline n = 25 cells, VPA n = 54 cells, t = 2.95, df = 77, \*\*P = 0.0042; P28: Saline n = 28 cells, VPA n = 42 cells, t = 2.04, df = 68, \*P = 0.0447; P35: Saline n = 42 cells, VPA n = 41 cells, t = 1.15, df = 81, P = 0.2517). **(m)** The total charge of sEPSCs per second recorded from pyramidal neurons in the mPFC of Saline and VPA mice at P21, P28 and P35 (P21: Saline n = 25 cells, VPA n = 51 cells, t = 2.28, df = 74, \*P = 0.0258; P28: Saline n = 28 cells, VPA n = 41 cells, t = 2.26, df = 67, \*P = 0.0273; P35: Saline n = 42 cells, VPA n = 40 cells, t = 2.26, df = 80, \*P = 0.0264). **n** Representative traces showing sIPSCs recorded from pyramidal neurons in the mPFC of Saline and VPA mice at P21, P28, and P35. **o** The average amplitude of sIPSCs recorded from pyramidal neurons in the mPFC of Saline and VPA mice at P21, P28 and P35 (P21: Saline n = 25 cells, VPA n = 54 cells, t = 0.47, df = 77, P = 0.6375; P28: Saline n = 28 cells, VPA n = 42 cells, t = 3.25, df = 68, \*\*\*P = 0.0018; P35: Saline n = 42 cells, VPA n = 41 cells, t = 0.04, df = 81, P = 0.9665). **p** The average frequency of sIPSCs recorded from pyramidal neurons in the mPFC of Saline and VPA mice at P21, P28 and P35 (P21: Saline n = 25 cells, VPA n = 54 cells, t = 0.25, df = 77, P = 0.8027; P28: Saline n = 28 cells, VPA n = 42 cells, t = 1.36, df = 68, P = 0.1771; P35: Saline n = 42 cells, VPA n = 41 cells, t = 1.01, df = 81, P = 0.3198). **q** The total charge of sIPSCs per second recorded from pyramidal neurons in the mPFC of Saline and VPA mice at P21, P28 and P35 (P21: Saline n = 25 cells, VPA n = 54 cells, t = 1.19, df = 77, P = 0.849; P28: Saline n = 28 cells, VPA n = 42 cells, t = 2.24, df = 68, \*P = 0.0286; P35: Saline n = 41 cells, VPA n = 41 cells, t = 2.06, df = 80, \*P = 0.0427). Data are represented as mean  $\pm$  SEM.

protein is down-regulated [31–34]. Previous studies that showed down-regulation of PV expression at the tissue level, such as western blotting, did not provide a precise answer to this question at the single-cell level. Some studies using immunostaining of PNN markers have shown no change in the number of PV<sup>+</sup> neurons in ASD animal models, such as shank mutant mice [33]. However, it should be noted that PNNs enwrap not only mature PV<sup>+</sup> neurons but also excitatory pyramidal neurons, which have been reported in the hippocampus [35]. Moreover, we also observed a considerable number of WFA<sup>+</sup>PV<sup>+</sup> neurons in the mPFC, as shown in Supplementary Fig. 5. Therefore, more reliable approaches and analysis are necessary to accurately answer this question.

In our study, we increased neuronal excitability by incubating acute brain slices in ACSF with high potassium concentration, and found that the expression of PV significantly was significantly enhanced. In contrast, by injecting AAV-hSyn-DIO-hM4Di-mCherry into the mPFC of PV-Cre mice, we were able to trace PV<sup>+</sup> neurons independent of PV immunoreactivity while down-regulating the activity of these neurons. We found when the expression of PV in individual PV<sup>+</sup> neuron was reduced due to decreased activity, the density of PV<sup>+</sup> neurons tagged by mCherry was not affected. Therefore, our results directly demonstrate that the expression level of PV is activity-dependent. Thus, increased activity of PV<sup>+</sup> neurons leads to PV<sub>L</sub>-to-PV<sub>H</sub> transition, and *vice versa*. Our data also implicate that it is the decreased expression of PV protein in individual PV<sup>+</sup> neuron, but not the decreased number of PV<sup>+</sup> neurons, that occurs in the developing mPFC in ASD. If PV<sub>H</sub> neurons do not receive enough inputs to maintain their activity, they may transit to PV<sub>L</sub> neurons. The number of visible PV<sup>+</sup> neurons appears to decrease when PV expression level in some PV<sup>+</sup> neurons falls below the detectable level by immunostaining. This may explain the decrease in the number of PV<sup>+</sup> neurons in previous studies [31, 32], and in our study that the total number of PV<sup>+</sup> neurons quantified by immunoreactivity was not altered at P21, but slightly decreased at P28 in VPA mice. Together, the

inconsistency in different studies may be due to the varying degrees of reduction in neuronal activity in different animal models of ASD or different experimental conditions.

#### Unchanged E/I ratio during postnatal development in ASD

While several studies have reported alterations in the E/I balance in various brain regions in ASD including V1 [36], S1 [37], and mPFC [38], our study did not observe a significant change in the E/I ratio from P21 to P35 in the mPFC of VPA mice, calculated using either spontaneous or evoked postsynaptic currents. The results we observed are consistent with the notion that if both cortical excitation and inhibition change in the same direction simultaneously, basal E/I balance may remain unchanged. Additional electrophysiological experiments are required to confirm whether spontaneous or evoked E/I ratio in the mPFC is altered in other ASD animal models. Nonetheless, our findings suggest that the alteration in basal E/I ratio in mPFC microcircuits during postnatal development may not be necessary for the neuropathogenesis of ASD.

#### Decreased excitation but not PV<sup>+</sup> interneuron-mediated inhibition in the mPFC drives cortical circuit dysfunction in ASD

PV<sup>+</sup> interneurons play an essential role in the synchronization of cortical activity, and there is a growing body of literature indicating their significant involvement in social behaviors [12]. However, most of these studies have focused on adult animals, leaving the causal link between PV<sup>+</sup> neurons and the neuropathogenesis of ASD-like social dysfunction uncertain. In our study, we observed a notable reduction in the activity of PV<sup>+</sup> neurons and a downward-shifted spectrum of PV expression. However, manipulating PV<sup>+</sup> neuron-mediated inhibitory activity in the developing mPFC did not successfully reproduce or rescue ASD-like social novelty deficit.

Previous studies have reported reduced excitatory activity in the mPFC of FXS mice [39, 40]. Recent evidence shows that enhancing the excitatory activity in the mPFC during postnatal development

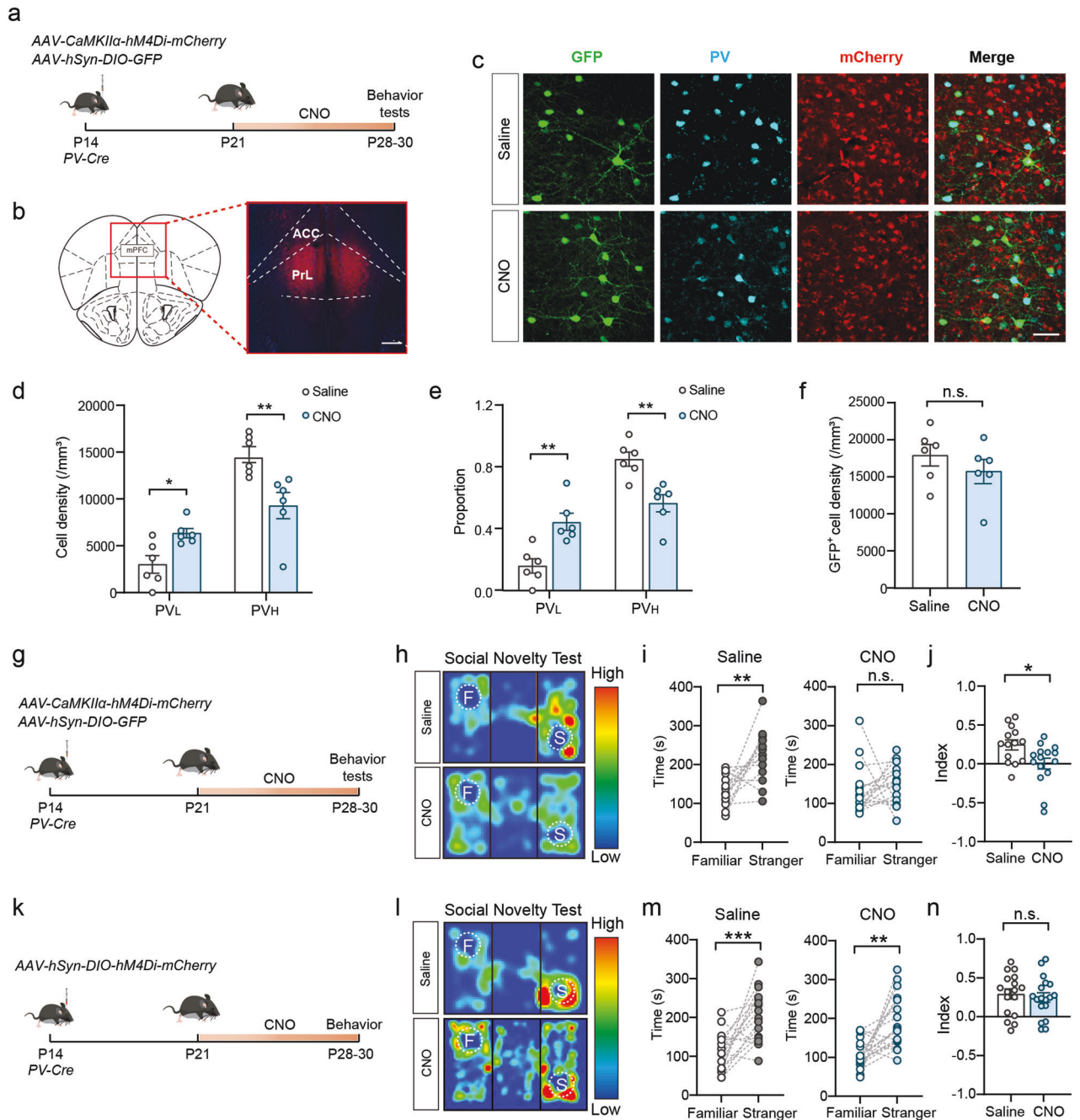


**Fig. 4** Decreased excitation but not PV<sup>+</sup> interneuron-mediated inhibition in the developing mPFC reproduced ASD-like social novelty deficit. **a** Schematics showing the chemogenetic approach to selectively suppressing the excitatory activity in the developing mPFC of PV-Cre mice. **b** Representative images showing the site of virus injection in the mPFC. Scale bar, 500  $\mu$ m. **c** Representative images showing the immunoreactivity of PV (cyan) in virally labeled PV<sup>+</sup> neurons (green) while manipulating the activity of excitatory neurons (mCherry) in the mPFC of PV-Cre mice. Scale bar, 50  $\mu$ m. **d** The density of PV<sub>H</sub> and PV<sub>L</sub> neurons in the mPFC of Saline- and CNO-treated mice (PV<sub>L</sub>: Saline n = 6 mice, CNO n = 6 mice,  $t = 3.14$ ,  $df = 10$ ,  $*P = 0.0105$ ; PV<sub>H</sub>: Saline n = 6 mice, CNO n = 6 mice,  $t = 3.33$ ,  $df = 10$ ,  $**P = 0.0076$ ). **e** The proportion of PV<sub>H</sub> and PV<sub>L</sub> neurons in the mPFC of Saline- and CNO-treated mice (PV<sub>L</sub>: Saline n = 6 mice, CNO n = 6 mice,  $t = 3.95$ ,  $df = 10$ ,  $**P = 0.0027$ ; PV<sub>H</sub>: Saline n = 6 mice, CNO n = 6 mice,  $t = 3.95$ ,  $df = 10$ ,  $**P = 0.0027$ ). **f** The density of total GFP-labeled PV<sup>+</sup> neurons in the mPFC of Saline- and CNO-treated mice (Saline: n = 6 mice, CNO: n = 6 mice,  $t = 1.01$ ,  $df = 10$ ,  $P = 0.338$ ). **g** Schematics showing selectively suppressing the excitatory activity in the developing mPFC of PV-cre mice. **h** Position heat map of Saline-treated (top) and CNO-treated (bottom) mice in social novelty test. **i** The time that Saline- or CNO-treated mice spent to interact with familiar and stranger mice (Saline: n = 14 mice, paired t-test,  $t = 3.97$ ,  $df = 13$ ,  $**P = 0.0016$ ; CNO: n = 16 mice, paired t-test,  $t = 0.135$ ,  $df = 15$ ,  $P = 0.8942$ ). **j** Social discrimination index of Saline- and CNO-treated mice (Saline: n = 14 mice, CNO: n = 16 mice,  $t = 2.374$ ,  $df = 28$ ,  $*P = 0.0247$ ). **k** Schematics showing selectively suppressing the inhibitory activity in the developing mPFC of PV-Cre mice. **l** Position heat map of Saline-treated (top) and CNO-treated (bottom) mice in social novelty test. **m** The time that Saline- or CNO-treated mice spent to interact with familiar and stranger mice (Saline: n = 17 mice, paired t-test,  $t = 4.31$ ,  $df = 16$ ,  $***P = 0.0005$ ; CNO: n = 18 mice, paired t-test,  $t = 3.691$ ,  $df = 17$ ,  $**P = 0.0018$ ). **n** Social discrimination index of Saline- and CNO-treated mice (Saline: n = 17 mice, CNO: n = 18 mice,  $t = 0.5017$ ,  $df = 33$ ,  $P = 0.6192$ ). Data are represented as mean  $\pm$  SEM.

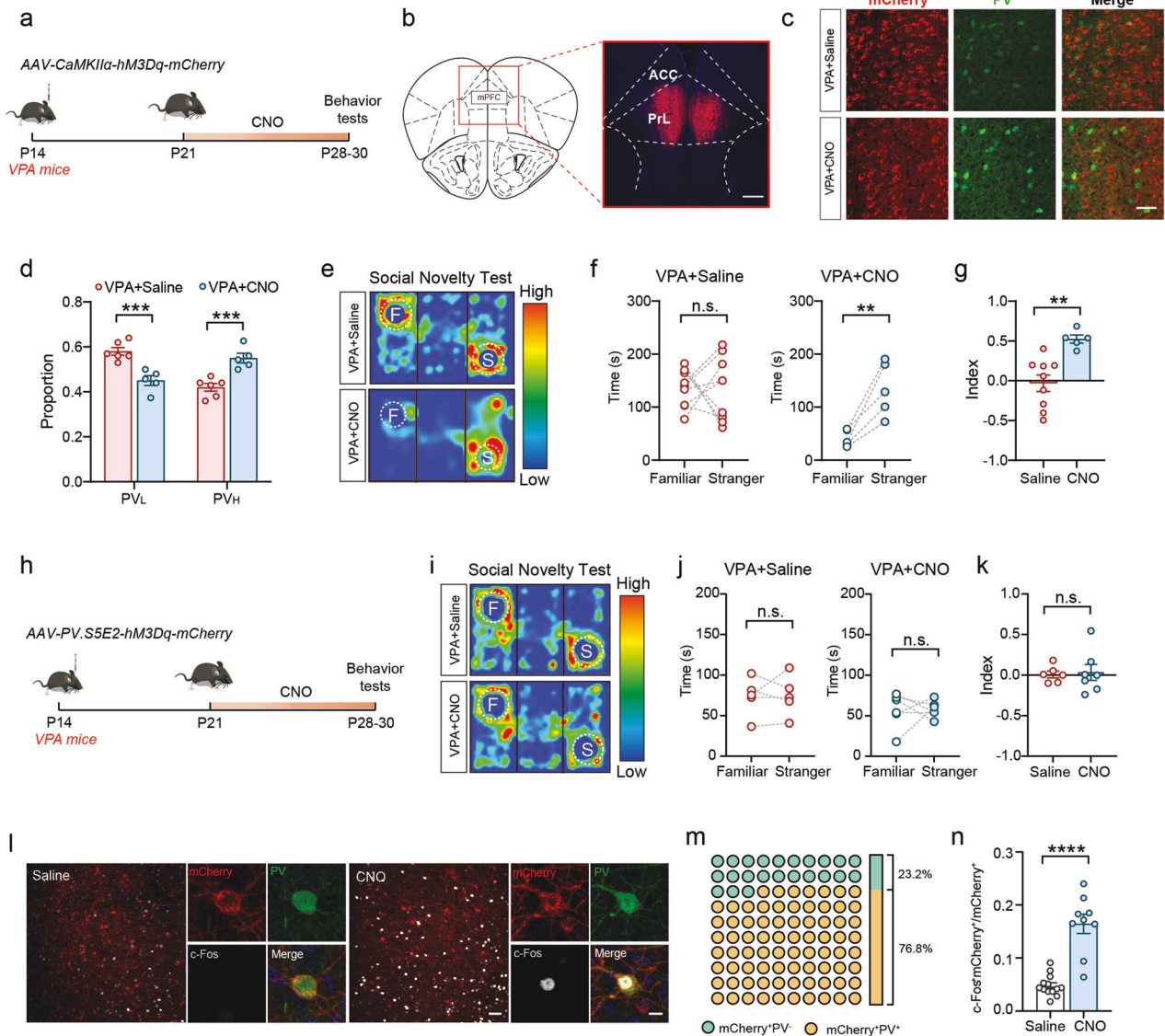


**Fig. 5** Enhancing excitation but not PV<sup>+</sup> interneuron-mediated inhibition in the developing mPFC rescued social deficit in VPA mice. **a** Schematics showing selectively enhancing the excitatory activity in the developing mPFC of VPA mice. **b** Representative image showing the site of virus injection in the mPFC. Scale bar, 500  $\mu$ m. **c** Representative images showing the immunoreactivity of PV (green) in the mPFC of Saline- and CNO-treated VPA mice. Excitatory neurons labeled by AAV expressing hM3Dq-mCherry (red). Scale bar, 50  $\mu$ m. **d** The proportion of PV<sub>H</sub> and PV<sub>L</sub> neurons in the mPFC of Saline- and CNO-treated VPA mice (PV<sub>L</sub>: Saline n = 6 mice, CNO n = 5 mice, t = 4.8, df = 9, \*\*\*P = 0.001; PV<sub>H</sub>: Saline n = 6 mice, CNO n = 5 mice, t = 4.8, df = 9, \*\*\*P = 0.001). **e** Position heat map of Saline-treated (top) and CNO-treated (bottom) VPA mice in social novelty test. **f** The time that Saline- or CNO-treated VPA mice spent to interact with familiar and stranger mice (Saline: n = 9 mice, paired t-test, t = 0.047, df = 8, P = 0.9639; CNO: n = 5 mice, paired t-test, t = 4.47, df = 4, \*\*P = 0.0088). **g** Social discrimination index of Saline- and CNO-treated VPA mice (Saline: n = 9 mice, VPA: n = 5 mice, t = 3.79, df = 12, \*\*P = 0.0026). **h** Schematics showing selectively enhancing the inhibitory activity in the developing mPFC of VPA mice. **i** Position heat map of Saline-treated (top) and CNO-treated (bottom) VPA mice in social novelty test. **j** The time that Saline- or CNO-treated VPA mice spent to interact with familiar and stranger mice (Saline: n = 5 mice, paired t-test, t = 0.13, df = 4, P = 0.9028; CNO: n = 5 mice, paired t-test, t = 0.069, df = 4, P = 0.948). **k** Social discrimination index of Saline- and CNO-treated VPA mice (Saline: n = 5 mice, VPA: n = 5 mice, t = 0.214, df = 8, P = 0.8344). Data are represented as mean  $\pm$  SEM. **l** Representative images showing the colocalization of PV (green) and c-Fos (gray) in neurons labeled by AAV-PV.S5E2-hM3Dq-mCherry (red) in Saline- or CNO-treated VPA mice. Scale: 50  $\mu$ m and 10  $\mu$ m (zoom in). **m** Majority of neurons labeled by AAV-PV.S5E2-hM3Dq-mCherry were PV<sup>+</sup>. **n** The proportion of c-Fos<sup>+</sup>mCherry<sup>+</sup> neurons in virus-labeled neurons after saline or CNO treatment (Saline: n = 13 mice, CNO: n = 9 mice, t = 7.093, df = 20, \*\*\*\*P < 0.0001).

can rescue impaired social functions in ASD animals such as contactin associated protein-like 2 (CNTNAP2)- and Abelson helper integration site-1 (AHI1)- knockdown mice [41]. Moreover, an autism-associated gene, *Scn2a*, is thought to contribute to the regulation of excitability of pyramidal neurons in the mPFC [42]. These clues point to the possibility that changes in cortical excitation in the developing mPFC may lead to impaired social

functions. However, it has not been directly demonstrated whether decreased excitatory activity in the mPFC during normal development can reproduce ASD-like social deficits in adulthood. In our study, we first found that the excitatory synaptic sites and activity-driven excitatory synaptic inputs in PV<sup>+</sup> neurons were both reduced in VPA mice, suggesting a decreased excitatory drive to mPFC PV<sup>+</sup> in ASD. Then we found that suppressing the

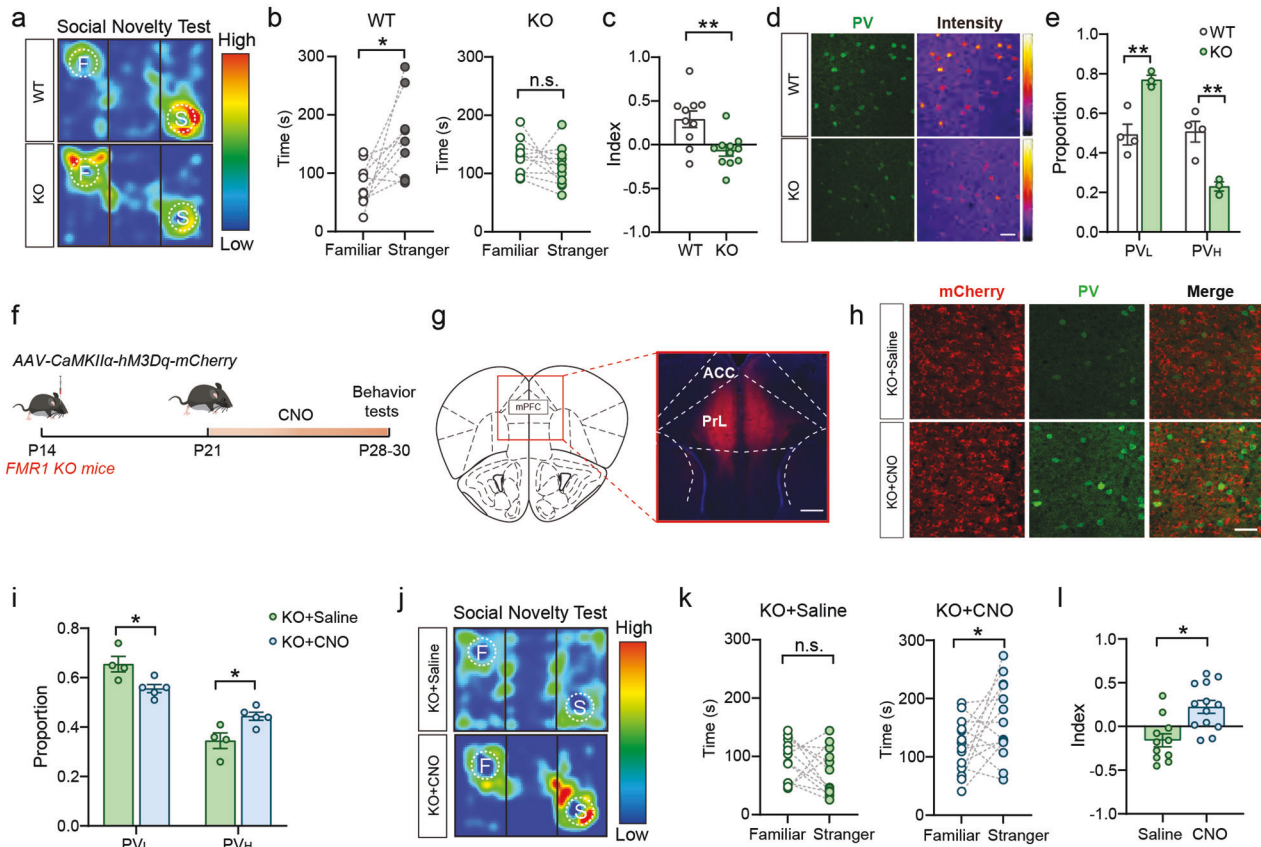


**Fig. 6** Enhancing excitation in the developing mPFC rescued social deficit in FMR1 KO mice. **a** Position heat map of WT (top) and FMR1 KO (bottom) mice in social novelty test. **b** The time that WT or FMR1 KO mice spent interacting with familiar and stranger mice (WT:  $n = 10$  mice, paired t-test,  $t = 2.8$ ,  $df = 9$ ,  $*P = 0.0206$ ; FMR1 KO:  $n = 11$  mice, paired t-test,  $t = 1.11$ ,  $df = 10$ ,  $P = 0.2933$ ). **c** Social discrimination index of WT and FMR1 KO mice (WT:  $n = 10$  mice, FMR1 KO:  $n = 11$  mice,  $t = 3.4$ ,  $df = 19$ ,  $**P = 0.003$ ). **d** Representative images showing PV immunoreactivity in the mPFC of WT and FMR1 KO mice at P21. Scale bar,  $50 \mu\text{m}$ . **e** The proportion of PV<sub>H</sub> and PV<sub>L</sub> neurons in the mPFC of WT and FMR1 KO mice (PV<sub>L</sub>: WT  $n = 4$  mice, KO  $n = 3$  mice,  $t = 4.24$ ,  $df = 5$ ,  $**P = 0.0082$ ; PV<sub>H</sub>: WT  $n = 4$  mice, KO  $n = 3$  mice,  $t = 4.24$ ,  $df = 5$ ,  $**P = 0.0082$ ). **f** Schematics showing selectively enhancing the excitatory activity in the developing mPFC of FMR1 KO mice. **g** Representative image showing the site of virus injection. Scale bar,  $500 \mu\text{m}$ . **h** Representative images showing the immunoreactivity of PV (green) in the mPFC of Saline-treated (top) and CNO-treated (bottom) FMR1 KO mice. Excitatory neurons labeled by AAV expressing hM3Dq-mCherry (red). Scale bar,  $50 \mu\text{m}$ . **i** The proportion of PV<sub>H</sub> and PV<sub>L</sub> neurons in the mPFC of Saline- and CNO-treated FMR1 KO mice (PV<sub>L</sub>: Saline  $n = 4$  mice, CNO  $n = 5$  mice,  $t = 2.99$ ,  $df = 7$ ,  $*P = 0.0201$ ; PV<sub>H</sub>: Saline  $n = 4$  mice, CNO  $n = 5$  mice,  $t = 2.99$ ,  $df = 7$ ,  $*P = 0.0201$ ). **j** Position heat map of Saline-treated (top) and CNO-treated (bottom) FMR1 KO mice in social novelty test. **k** The time that Saline- or CNO-treated FMR1 KO mice spent to interact with familiar and stranger mice (Saline:  $n = 12$  mice, paired t-test,  $t = 1.294$ ,  $df = 11$ ,  $P = 0.2222$ ; CNO:  $n = 15$  mice, paired t-test,  $t = 2.353$ ,  $df = 14$ ,  $*P = 0.0338$ ). **l** Social discrimination index of Saline- and CNO-treated FMR1 KO mice (Saline:  $n = 12$  mice, CNO:  $n = 15$  mice,  $t = 2.6$ ,  $df = 25$ ,  $*P = 0.0154$ ). Data are represented as mean  $\pm$  SEM.

excitation in the developing mPFC of wild-type mice reproduced ASD-like social novelty deficit. Conversely, by enhancing the excitation in ASD mice, we were able to rescue their social novelty deficit. These findings strongly suggest that alterations in cortical excitation during postnatal development may play a critical role in mediating social dysfunction in ASD.

Together, our data provide several new insights into the role of excitatory activity and PV<sup>+</sup> interneurons in ASD-like social cognitive dysfunction: (1) we found that changes in excitatory activity occur before alterations in inhibitory activity in the developing mPFC of ASD mice; (2) excitatory synaptic inputs have a significant impact on the activity state and PV expression of PV<sup>+</sup> neurons; and (3) manipulating excitatory activity in the developing mPFC reproduce or rescue ASD-like social novelty deficit, while manipulating PV<sup>+</sup> interneuron-mediated inhibitory activity does not produce the same effects. These findings suggest that decreased excitation, rather than PV<sup>+</sup> interneuron-mediated inhibition, during postnatal development serves as the primary driver of cortical microcircuit dysfunction within the mPFC. This dysfunction ultimately leads to

impaired social cognition in ASD. It is important to note that altered inhibition may still play a role at later stages of development, but our results highlight the critical role of decreased excitation in the early neuropathogenesis of impaired social cognition in ASD.

#### Time windows for treating ASD by manipulating cortical excitatory activity

There is growing evidence to support the hypothesis that ASD is a neurodevelopmental disorder with sensitive time windows [43, 44]. Indeed, in this study, we manipulated cortical excitation in a narrow time window (P21 to P28) in the developing mPFC, and found that selectively suppressing excitation during this period mimicked ASD-like social deficits. More importantly, enhancing excitation during this period successfully rescued social deficits in ASD mice. These findings not only suggest a common cellular mechanism underlying the neuropathogenesis in different ASD animal models, such as VPA or FMR1 KO mice, but also highlight a potential target and a unique developmental window for intervention in both environmentally and genetically induced ASD. Overall, our data

contribute to our understanding of critical time windows for cortical microcircuit development and have significant implications for early intervention in the treatment of ASD.

## DATA AVAILABILITY

All data presented in this study are included in this article and its supplementary files.

## REFERENCES

- Willsey HR, Willsey AJ, Wang B, State MW. Genomics, convergent neuroscience and progress in understanding autism spectrum disorder. *Nat Rev Neurosci*. 2022;23:323–41.
- Galineau L, Arlicot N, Dupont AC, Briend F, Houy-Durand E, Tauber C, et al. Glutamatergic synapse in autism: a complex story for a complex disorder. *Mol Psychiatry*. 2023;28:801–9.
- Coghlan S, Horder J, Inkster B, Mendez MA, Murphy DG, Nutt DJ. GABA system dysfunction in autism and related disorders: from synapse to symptoms. *Neurosci Biobehav Rev*. 2012;36:2044–55.
- Fortier AV, Meisner OC, Nair AR, Chang SWC. Prefrontal circuits guiding social preference: implications in autism spectrum disorder. *Neurosci Biobehav Rev*. 2022;141:104803.
- Zikopoulos B, Barbas H. Altered neural connectivity in excitatory and inhibitory cortical circuits in autism. *Front Hum Neurosci*. 2013;7:609.
- Rubenstein JL, Merzenich MM. Model of autism: increased ratio of excitation/inhibition in key neural systems. *Genes Brain Behav*. 2003;2:255–67.
- Nelson SB, Valakh V. Excitatory/inhibitory balance and circuit homeostasis in autism spectrum disorders. *Neuron*. 2015;87:684–98.
- Melillo R, Leisman G. Autistic spectrum disorders as functional disconnection syndrome. *Rev Neurosci*. 2009;20:111–31.
- Bicks LK, Koike H, Akbarian S, Morishita H. Prefrontal cortex and social cognition in mouse and man. *Front Psychol*. 2015;6:1805.
- Grossmann T. The role of medial prefrontal cortex in early social cognition. *Front Hum Neurosci*. 2013;7:340.
- Chini M, Hanganu-Opatz IL. Prefrontal cortex development in health and disease: lessons from rodents and humans. *Trends Neurosci*. 2021;44:227–40.
- Ferguson BR, Gao WJ. PV interneurons: critical regulators of E/I balance for prefrontal cortex-dependent behavior and psychiatric disorders. *Front Neural Circuits*. 2018;12:37.
- Amina S, Falcone C, Hong T, Wolf-Ochoa MW, Vakilzadeh G, Allen E, et al. Chandelier cartridge density is reduced in the prefrontal cortex in autism. *Cereb Cortex*. 2021;31:2944–51.
- Wohr M, Orduz D, Gregory P, Moreno H, Khan U, Vorckel KJ, et al. Lack of parvalbumin in mice leads to behavioral deficits relevant to all human autism core symptoms and related neural morphofunctional abnormalities. *Transl Psychiatry*. 2015;5:e525.
- Tyzio R, Nardou R, Ferrari DC, Tsintsadze T, Shahrokhi A, Eftekhari S, et al. Oxytocin-mediated GABA inhibition during delivery attenuates autism pathogenesis in rodent offspring. *Science*. 2014;343:675–9.
- Wojtowicz JM, Kee N. BrdU assay for neurogenesis in rodents. *Nat Protoc*. 2006;1:1399–405.
- Rein B, Ma K, Yan Z. A standardized social preference protocol for measuring social deficits in mouse models of autism. *Nat Protoc*. 2020;15:3464–77.
- del Rio JA, de Lecea L, Ferrer I, Soriano E. The development of parvalbumin-immunoreactivity in the neocortex of the mouse. *Brain Res. Dev Brain Res*. 1994;81:247–59.
- Donato F, Rompani SB, Caroni P. Parvalbumin-expressing basket-cell network plasticity induced by experience regulates adult learning. *Nature*. 2013;504:272–6.
- Donato F, Chowdhury A, Lahr M, Caroni P. Early- and late-born parvalbumin basket cell subpopulations exhibiting distinct regulation and roles in learning. *Neuron*. 2015;85:770–86.
- Miranda JM, Cruz E, Bessieres B, Alberini CM. Hippocampal parvalbumin interneurons play a critical role in memory development. *Cell Rep*. 2022;41:111643.
- Sigal YM, Bae H, Bogart LJ, Hensch TK, Zhuang X. Structural maturation of cortical perineuronal nets and their perforating synapses revealed by superresolution imaging. *Proc Natl Acad Sci USA*. 2019;116:7071–6.
- Christensen J, Gronborg TK, Sorensen MJ, Schendel D, Parner ET, Pedersen LH, et al. Prenatal valproate exposure and risk of autism spectrum disorders and childhood autism. *JAMA*. 2013;309:1696–703.
- Nicolini C, Fahnstocck M. The valproic acid-induced rodent model of autism. *Exp Neurol*. 2018;299:217–27.
- Zhao H, Wang Q, Yan T, Zhang Y, Xu HJ, Yu HP, et al. Maternal valproic acid exposure leads to neurogenesis defects and autism-like behaviors in non-human primates. *Transl Psychiatry*. 2019;9:267.
- Roulet FJ, Lai JK, Foster JA. In utero exposure to valproic acid and autism—a current review of clinical and animal studies. *Neurotoxicol Teratol*. 2013;36:47–56.
- Vormstein-Schneider D, Lin JD, Pelkey KA, Chittajallu R, Guo B, Arias-Garcia MA, et al. Viral manipulation of functionally distinct interneurons in mice, non-human primates and humans. *Nat Neurosci*. 2020;23:1629–36.
- Spencer CM, Alekseyenko O, Serysheva E, Yuva-Paylor LA, Paylor R. Altered anxiety-related and social behaviors in the Fmr1 knockout mouse model of fragile X syndrome. *Genes Brain Behav*. 2005;4:420–30.
- Peier AM, McLwain KL, Kenneson A, Warren ST, Paylor R, Nelson DL. (Over)correction of FMR1 deficiency with YAC transgenics: behavioral and physical features. *Hum Mol Genet*. 2000;9:1145–59.
- Lim L, Mi D, Llorca A, Marin O. Development and functional diversification of cortical interneurons. *Neuron*. 2018;100:294–313.
- Hashemi E, Ariza J, Rogers H, Noctor SC, Martinez-Cerdeno V. The number of parvalbumin-expressing interneurons is decreased in the prefrontal cortex in autism. *Cereb Cortex*. 2017;27:1931–43.
- Ariza J, Rogers H, Hashemi E, Noctor SC, Martinez-Cerdeno V. The number of chandelier and basket cells are differentially decreased in prefrontal cortex in autism. *Cereb Cortex*. 2018;28:411–20.
- Filice F, Vorckel KJ, Sungur AO, Wohr M, Schwaller B. Reduction in parvalbumin expression not loss of the parvalbumin-expressing GABA interneuron subpopulation in genetic parvalbumin and shank mouse models of autism. *Mol Brain*. 2016;9:10.
- Lauber E, Filice F, Schwaller B. Dysregulation of parvalbumin expression in the Cntnap2<sup>-/-</sup> mouse model of autism spectrum disorder. *Front Mol Neurosci*. 2018;11:262.
- Carstens KE, Phillips ML, Pozzo-Miller L, Weinberg RJ, Dudek SM. Perineuronal nets suppress plasticity of excitatory synapses on CA2 pyramidal neurons. *J Neurosci*. 2016;36:6312–20.
- Del Rosario J, Speed A, Arrowood H, Motz C, Pardue M, Haider B. Diminished cortical excitation and elevated inhibition during perceptual impairments in a mouse model of autism. *Cereb Cortex*. 2021;31:3462–74.
- Antoine MW, Langberg T, Schnepel P, Feldman DE. Increased excitation-inhibition ratio stabilizes synapse and circuit excitability in four autism mouse models. *Neuron*. 2019;101:648–661 e644.
- Yizhar O, Fenno LE, Prigge M, Schneider F, Davidson TJ, O’Shea DJ, et al. Neocortical excitation/inhibition balance in information processing and social dysfunction. *Nature*. 2011;477:171–8.
- Krueger DD, Osterweil EK, Chen SP, Tye LD, Bear MF. Cognitive dysfunction and prefrontal synaptic abnormalities in a mouse model of fragile X syndrome. *Proc Natl Acad Sci USA*. 2011;108:2587–92.
- Hwang JY, Monday HR, Yan J, Gompers A, Buxbaum AR, Sawicka KJ, et al. CPEB3-dependent increase in GluA2 subunits impairs excitatory transmission onto inhibitory interneurons in a mouse model of fragile X. *Cell Rep*. 2022;39:110853.
- Sacai H, Sakoori K, Konno K, Nagahama K, Suzuki H, Watanabe T, et al. Autism spectrum disorder-like behavior caused by reduced excitatory synaptic transmission in pyramidal neurons of mouse prefrontal cortex. *Nat Commun*. 2020;11:5140.
- Spratt PWE, Ben-Shalom R, Keeshen CM, Burke KJ Jr, Clarkson RL, Sanders SJ, et al. The autism-associated gene Scn2a contributes to dendritic excitability and synaptic function in the prefrontal cortex. *Neuron*. 2019;103:673–685 e675.
- LeBlanc JJ, Fagioli M. Autism: a “critical period” disorder? *Neural Plast*. 2011;2011:921680.
- Meredith RM. Sensitive and critical periods during neurotypical and aberrant neurodevelopment: a framework for neurodevelopmental disorders. *Neurosci Biobehav Rev*. 2015;50:180–8.

## ACKNOWLEDGEMENTS

We thank all the members of the YG and Lang W laboratories for the discussion and meaningful suggestions for this project. We are grateful to the Core Facilities of Zhejiang University School of Medicine for technique assistance.

## AUTHOR CONTRIBUTIONS

YL, Liang W, YG, and Lang W designed all the experiments; YL and Liang W conducted most of the experiments, including most imaging, viral injection, electrophysiology, behavioral experiments, and related analysis; YC prepared some VPA mice and did some imaging analysis; YS provided Fmr1-KO mouse line; YL, Liang W, YG, and Lang W discussed the results and wrote the manuscript. All authors read and discussed about the manuscript.

## FUNDING

This work was supported by grants from STI2030-Major Projects 2021ZD0204000 (2021ZD0204003 to LW), the Zhejiang Provincial Natural Science Foundation (LR21C090001), the National Natural Science Foundation of China (32070975) to LW, the National Science Fund for Distinguished Young Scholars (32225021), the National Natural Science Foundation of China (32071021) to YG, and the National Natural Science Foundation of China (31820103005) to YS. This work was also supported by the MOE Frontier Science Center for Brain Science & Brain-Machine Integration, Zhejiang University, and the Fundamental Research Funds for the Central Universities (2023ZFJH01-01, 2024ZFJH01-01).

## COMPETING INTERESTS

The authors declare no competing interests.

## ADDITIONAL INFORMATION

**Supplementary information** The online version contains supplementary material available at <https://doi.org/10.1038/s41398-024-03043-2>.

**Correspondence** and requests for materials should be addressed to Yan Gu or Lang Wang.

**Reprints and permission information** is available at <http://www.nature.com/reprints>

**Publisher's note** Springer Nature remains neutral with regard to jurisdictional claims in published maps and institutional affiliations.



**Open Access** This article is licensed under a Creative Commons Attribution-NonCommercial-NoDerivatives 4.0 International License, which permits any non-commercial use, sharing, distribution and reproduction in any medium or format, as long as you give appropriate credit to the original author(s) and the source, provide a link to the Creative Commons licence, and indicate if you modified the licensed material. You do not have permission under this licence to share adapted material derived from this article or parts of it. The images or other third party material in this article are included in the article's Creative Commons licence, unless indicated otherwise in a credit line to the material. If material is not included in the article's Creative Commons licence and your intended use is not permitted by statutory regulation or exceeds the permitted use, you will need to obtain permission directly from the copyright holder. To view a copy of this licence, visit <http://creativecommons.org/licenses/by-nc-nd/4.0/>.

© The Author(s) 2024